
A PAC-Bayesian View of Generalisation for Physics-Informed Machine Learning

Thien V. Nguyen

Université Jean Monnet Saint-Étienne, CNRS, Institut d'Optique Graduate School,
Laboratoire Hubert Curien UMR 5516, F-42023, Saint-Étienne, France
van.thien.nguyen@univ-st-etienne.fr

Amaury Habrard

Université Jean Monnet Saint-Étienne, CNRS, Institut d'Optique Graduate School,
Laboratoire Hubert Curien UMR 5516, Inria, F-42023, Saint-Étienne, France
Institut Universitaire de France
amaury.habrard@univ-st-etienne.fr

Benjamin Guedj

Inria and University College London,
France and United Kingdom
b.guedj@ucl.ac.uk

Abstract

Physics-informed machine learning (PIML) integrates mechanistic knowledge, typically in the form of partial differential equations (PDE), into data-driven models. Despite strong empirical performance, its statistical generalisation properties remain poorly understood, particularly in the regression setting with unbounded losses. Existing analyses rely on approximation or stability arguments and do not fully capture how physical structure influences generalisation from finite data. In this work, we develop a PAC-Bayesian framework for PIML that provides high-probability generalisation guarantees in the presence of unbounded losses. We adopt a multi-task perspective that jointly treats data fidelity, PDE residuals, initial and boundary conditions, avoiding the looseness induced by standard union-bound approaches. Our analysis leverages the structure of physics-informed objectives to derive novel bounds where the complexity scales with input-gradient norms of the losses, revealing a direct link between physical regularity and generalisation. We instantiate this framework under Sobolev and Poincaré-type assumptions, yielding two classes of bounds that trade off statistical complexity and smoothness in different regimes. Building on these results, we propose a self-bounding-aware learning algorithm that directly optimises tractable surrogates of the derived bounds, along with a practical procedure to estimate the associated constants in realistic settings. Empirical evaluations on standard PDE benchmarks demonstrate that our bounds are non-vacuous, significantly tighter than union-bound baselines, and can be effectively minimised during training. Overall, our results provide a principled statistical foundation for the generalisation of physics-informed models.

1 Introduction

Physics-informed machine learning [PIML, 25] aims to integrate prior scientific knowledge, typically expressed as partial differential equations (PDEs), into data-driven models. By constraining the hypothesis space through physical laws, PIML has demonstrated strong empirical performance across

a range of applications, including forward and inverse problems, scientific simulation, and hybrid modelling. A central premise underlying these methods is that physical structure should improve generalisation by reducing the effective complexity of the learned model.

Despite this intuition, the statistical mechanisms by which physical constraints influence generalisation remains poorly understood. Existing theoretical analyses of PIML largely focus on approximation error or optimisation behaviour, and only partially address the fundamental statistical question: how well does a model trained on finite data generalise to unseen inputs? This gap is particularly pronounced in realistic settings, where losses are unbounded and multiple heterogeneous objectives (data fidelity, PDE residuals, and boundary conditions) are optimised jointly.

Among the most prominent approaches, physics-informed neural networks (PINNs) [32] enforce physical constraints by penalising violations of the governing equations during training, while alternative formulations based on kernel methods [11] and variational principles [34] have recently gained attention. However, the theoretical understanding of generalisation capabilities of PIML methods remains a challenging issue. A large spectrum of results studied the difficulty of learning PINNs establishing convergence rates [38, 12]. [35, 28] proposed a general schema for deriving generalisation bounds based on stability properties and approximation results. Some paper have studied generalisation based on (local) Rademacher complexity [24, 26, 42]. Related works are discussed in Appendix D.

In this paper, we provide a novel view of the PIML problem through PAC-Bayes theory [1, 17, 22]. This theory provides a powerful framework to study model performance considering randomised predictors and establishing robust, flexible generalisation guarantees. A central feature of this framework is the trade-off between empirical performance and model complexity, typically quantified via an information-theoretic divergence between a data-dependent posterior distribution and a prior. This perspective is particularly appealing for PIML, as it enables the integration of physical knowledge in the form of structured priors or constraints on the hypothesis space.

However, applying PAC-Bayes tools to PIML raises significant challenges. Early PAC-Bayesian works concentrate on bounded losses for classification, whereas PIML is inherently a regression framework with unbounded loss functions (for example, squared error or the residual of a differential operator) that can exhibit complex tail behavior. Consequently, standard PAC-Bayes bounds, whose derivations typically rely on boundedness assumptions or sub-Gaussian tails, do not apply directly. Extending PAC-Bayesian guarantees to this PIML regime therefore requires controlling exponential moments of potentially heavy-tailed losses, a non-trivial task that requires additional structural assumptions like assuming boundedness of higher-order moments of the loss [19, 23], or of the cumulant generating function (CGF) [6, 33]. However, these assumptions introduce new parameters or constants that are difficult to estimate or optimise in practice, and their connections to the bound, the data, or the underlying physical constraints remain less intuitive.

In this work, we address this gap by developing PAC-Bayesian generalisation bounds tailored to physics-informed learning in regression settings with unbounded losses. Our approach explicitly accounts for the hybrid nature of PIML, where the learning objective combines a data-fitting term and a physics-based regularisation term encoding prior knowledge through a differential operator. We show how this structure can be leveraged within the PAC-Bayesian framework to derive meaningful generalisation guarantees going beyond the classical bounded-loss setting. In particular, we provide bounds that capture the interplay between data, model complexity, and the strength of the physical prior, thereby offering new insights into when and how physics improves learning.

Our key insight is that PIML admits a natural multi-task structure in which data and physics constraints can be treated jointly within a single PAC-Bayesian analysis. Exploiting this structure allows us to derive significantly tighter bounds than standard approaches based on independent treatment of each loss. Moreover, we show that the interaction between physical constraints and generalisation can be captured through input-gradient dependent complexity terms, revealing a direct connection between the smoothness induced by physics and statistical performance.

Our contribution are as follows:

- We treat the PIML problem from a multi-task point of view and propose two different smoothness assumptions, namely Sobolev 3.3 (stronger) and Poincaré 3.6 (weaker), to derive two new bounds (Theorem 3.5 and Theorem 3.7) where the complexity scales with the weighted norm of the gradient of the losses with respect to (w.r.t) the input.

- To complement our theory, we examine the practical plausibility of the underlying assumptions by means of a principled procedure to estimate the Sobolev and Poincaré constants to reflect real model and data distributions. Using these estimators, we present a self-bounding PIML that directly targets the derived generalisation bounds by minimising their stochastic surrogate objectives, yielding a practical training procedure that aligns optimisation with the theoretical guarantees.
- We evaluate our algorithm and the associated generalisation bounds on PDE benchmarks. Results show that our bounds are substantially tighter than classic union-bound baselines, and that the self-bounding procedure reliably reduces the bound in practice. Interestingly, we show that informed priors can be built by exploiting only the PDE structure on the input domain—without additional labeled data to learn the prior—thereby improving bound tightness while staying label-efficient.

2 Preliminaries

2.1 Physics-informed machine learning

A PDE with equation constraints, initial (ICs) and boundary conditions (BCs) can be formulated as

$$\mathcal{D}[u](\mathbf{x}) = 0, \mathbf{x} \in \Omega; \quad \mathcal{I}[u](0, \mathbf{x}) = 0, \mathbf{x} \in \Omega_0; \quad \mathcal{B}[u](\mathbf{x}) = 0, \mathbf{x} \in \partial\Omega, \quad (1)$$

where $\mathcal{D}, \mathcal{I}, \mathcal{B}$ are (residual) derivative, initial and boundary operators, respectively. The aim is to learn the target function $u : \mathbb{R}^d \rightarrow \mathbb{R}$, which maps an input vector $\mathbf{x} \in \Omega \subset \mathbb{R}^d$ to an output value $y \in \mathbb{R}$. Here $\mathbf{x} \in \mathbb{R}^d$ stands for the input coordinate, composed of time and spatial position. Ω_0 corresponds to the $t = 0$ instance, while $\partial\Omega$ corresponds to extreme spatial positions. Our goal is to learn a parametric model u_θ that approximates the true function u , with $\theta \in \mathbb{R}^d$ a parameter set belonging to a model class Θ . As an abuse of notation $\theta \in \Theta$ designs both a model and its parameters with $d_\theta := d$, we also assume that u_θ belongs to the Sobolev Space $H^1(\Omega)$. Typically, learning is done by minimising the following physics-informed machine learning risk:

$$\begin{aligned} \hat{\mathcal{R}}_{\text{PIML}_\lambda}(\theta) &= \lambda_d \hat{\mathcal{R}}_d(\theta) + \lambda_p \hat{\mathcal{R}}_p(\theta) + \lambda_{ic} \hat{\mathcal{R}}_{ic}(\theta) + \lambda_{bc} \hat{\mathcal{R}}_{bc}(\theta) \\ &= \frac{\lambda_d}{|S_d|} \sum_{(\mathbf{x}, y) \in S_d} \ell_d(u_\theta(\mathbf{x}), y) + \frac{\lambda_p}{|S_p|} \sum_{\mathbf{x} \in S_p} \ell_p(\mathcal{D}[u_\theta](\mathbf{x})) \\ &\quad + \frac{\lambda_{ic}}{|S_{ic}|} \sum_{\mathbf{x} \in S_{ic}} \ell_{ic}(\mathcal{I}[u_\theta](\mathbf{x})) + \frac{\lambda_{bc}}{|S_{bc}|} \sum_{\mathbf{x} \in S_{bc}} \ell_{bc}(\mathcal{B}[u_\theta](\mathbf{x})), \end{aligned} \quad (2)$$

where $\ell_d, \ell_p, \ell_{ic}, \ell_{bc}$ are data-fidelity, PDE, IC and BC loss functions, respectively. Note that $\ell_p, \ell_{ic}, \ell_{bc}$ are the physics-based loss terms. We let S_d, S_p, S_{ic}, S_{bc} be the corresponding sets of observation and PDE, IC, BC collocation points, **drawn independent across datasets and i.i.d within each dataset**. We consider a flexible framework where each sample can be generated by a different probability distribution, modeling potentially diverse acquisitions procedures. Note that S_d is generated over $\Omega \times \mathbb{R}$, while the others are generated over Ω . For convenience, we use an abuse of notation using generic losses $\ell_i(\theta, \mathbf{x})$ where \mathbf{x} denotes either a data from $\Omega \times \mathbb{R}$ or Ω depending the loss considered, however the input gradient $\nabla_{\mathbf{x}} \ell_i(\theta, \mathbf{x})$ is always considered with respect to the input space Ω . The hyperparameters $\lambda_d, \lambda_p, \lambda_{ic}, \lambda_{bc}$ control the relative importance of these loss terms. This formulation encourages the learned model to not only match the observed data, but also to remain consistent with the underlying physical laws encoded by the PDE. **It can be seen as a particular multi-task problem with a shared backbone and deterministic, non-learned heads determined by the governing PDE system**. Hence, to streamline the subsequent theoretical analysis, we consider a physics-informed optimisation problem comprising N_L loss components, where the i -th component is ℓ_i and is trained on a dataset S_i sampled from an underlying distribution D_i . Besides, for an arbitrary loss function ℓ , denote $\mathcal{R}(\theta) = \mathbb{E}_{\mathbf{x}} \ell(\theta, \mathbf{x})$ and $\hat{\mathcal{R}}(\theta) = \frac{1}{|S|} \sum_{\mathbf{x} \in S} \ell(\theta, \mathbf{x})$ as its population (true) and empirical risk on its training set S . This way, we can rewrite the weighted empirical PIML risk above as $\hat{\mathcal{R}}_{\text{PIML}_\lambda}(\theta) = \sum_{i=1}^{N_L} \lambda_i \hat{\mathcal{R}}_i(\theta)$.

Training PINNs is challenging and typically requires adapting the loss weights $\{\lambda_i\}$ to improve convergence [27, 41], which yields different $\{\lambda_i\}$ across runs even for the same training data. Consequently, it is inappropriate to rely on these adaptively weighted risks when studying the generalisation of the learned model. The simplest alternative is to consider the total risk $\mathcal{R}_{\text{PIML}}(\theta) = \sum_{i=1}^{N_L} \mathcal{R}_i(\theta)$. Besides, in a general multi-task learning scenario, we have to deal with diverse training

sizes, therefore it might be of great interest to have also a sample-weighted risk (i.e., inspired by [43]) $\mathcal{R}_{\text{PIML}}^S(\boldsymbol{\theta}) = \frac{1}{M} \sum_{i=1}^{N_L} m_i \mathcal{R}_i(\boldsymbol{\theta})$, where m_i is the sample size of the i -th task and $M = \sum_{i=1}^{N_L} m_i$ is the total sample size. For convenience, let $S = \{S_i\}_{i=1}^{N_L}$ is the collection of training sets in PIML context. From these notions, we will consider two corresponding versions of generalisation gap:

$$\text{gen}(\boldsymbol{\theta}, S) = \mathcal{R}_{\text{PIML}}(\boldsymbol{\theta}) - \hat{\mathcal{R}}_{\text{PIML}}(\boldsymbol{\theta}) = \sum_{i=1}^{N_L} \frac{1}{m_i} \sum_{j=1}^{m_i} (\mathcal{R}_i(\boldsymbol{\theta}) - \ell_i(\boldsymbol{\theta}, \mathbf{x}_{i,j})), \quad (3)$$

$$\text{gen}^S(\boldsymbol{\theta}, S) = \mathcal{R}_{\text{PIML}}^S(\boldsymbol{\theta}) - \hat{\mathcal{R}}_{\text{PIML}}^S(\boldsymbol{\theta}) = \frac{1}{M} \sum_{i=1}^{N_L} \sum_{j=1}^{m_i} (\mathcal{R}_i(\boldsymbol{\theta}) - \ell_i(\boldsymbol{\theta}, \mathbf{x}_{i,j})). \quad (4)$$

2.2 PAC-Bayes bounds for regression

Recent advances [2, 19, 20] in PAC-Bayesian theory have removed a key restriction of classical generalisation guarantees by extending them to regression settings with unbounded losses, enabling PAC-Bayes analyses for a broader class of loss functions. These developments make the bounds finite even when individual losses are unbounded, thereby widening the theory’s applicability.

Bounds with KL divergence

A line of work builds on the variational representation of the Kullback–Leibler (KL) divergence to obtain PAC-Bayes bounds that accommodate heavier tails. [3] presents an oracle bound with a complexity term $\frac{1}{\lambda m} \left[\text{KL}(\rho \parallel \pi) + \ln \frac{\Psi_{P,D}(\lambda)}{\delta} \right]$ for a fixed λ , where ρ and π are respectively the posterior and prior distributions belonging to $\mathcal{M}(\Theta)$ the set of probability measures over the hypothesis class Θ ; and $\Psi_{\rho,D}(\lambda) := \mathbb{E}_{\boldsymbol{\theta} \sim \rho} \mathbb{E}_{S \sim D^m} \left[\exp(\lambda m (\mathcal{R}(\boldsymbol{\theta}) - \hat{\mathcal{R}}(\boldsymbol{\theta}))) \right]$. In the following, we assume ρ to be absolutely continuous with respect to π , and π to be independent from learning data that may be used to train ρ . To turn this oracle-style statement into practical data-dependent bounds, one must control the moment generating behavior of the loss. Prior works obtain such control under various tail assumptions [2, 7, 15], or by assuming a bounded CGF [33]. An alternative is to impose assumptions on the data distribution itself often cast as a Gaussian distribution [18, 37].

A practical complication is that many of these bounds depend on a tuning parameter λ that must be fixed independently of the training data. Early solutions grid over λ and apply a union bound, but this does not guarantee an optimal choice of λ . More recent work [6] uses a Cramér–Chernoff argument together with the generalised inverse to produce bounds that hold uniformly over $\lambda > 0$. The analysis is centered on the CGF $\Lambda_{\boldsymbol{\theta}}(\lambda) := \ln \mathbb{E}_{\mathbf{x} \sim D} [e^{\lambda(\mathcal{R}(\boldsymbol{\theta}) - \ell(\boldsymbol{\theta}, \mathbf{x}))}]$, and yields a complexity $\inf_{\lambda} \left[\frac{\text{KL}(\rho \parallel \pi) + \ln \frac{m}{\delta}}{\lambda(m-1)} + \frac{\mathbb{E}_{\boldsymbol{\theta} \sim Q} [\Lambda_{\boldsymbol{\theta}}(\lambda)]}{\lambda} \right]$, hence enabling us to conveniently solve for optimal λ .

Following prior work, [6] introduces model-dependent assumptions that allow one to solve for the λ minimising the above complexity term and obtain explicit bounds. As an example, they consider regularisation based on the model’s input gradient under a log-Sobolev type condition, $\Lambda_{\boldsymbol{\theta}}(\lambda) \leq \frac{C}{2} \lambda^2 \|\nabla_{\mathbf{x}} \ell\|_2^2$, which produces a bound with a *multiplicative complexity term*: the KL divergence is scaled by a hypothesis-dependent factor derived from the gradient norm.

Beyond KL divergence

The variational KL representation is not the only route to PAC-Bayes change-of-measure inequalities. Several recent works develop bounds using alternative divergences: Rényi divergences [5], f -divergences [2, 29, 31], or Wasserstein distance [40], among others. The work from [29] introduces several change-of-measure tools and applies them to different loss classes. One consequence is a multiplicative-complexity bound on the second-order moment of the loss as follows.

Theorem 2.1 (Generalised from Ohnisi and Honorio [29]). *For any confidence level $\delta \in (0, 1)$, any prior $\pi \in \mathcal{M}(\Theta)$, for any posterior $\rho \in \mathcal{M}(\Theta)$, with probability at least $1 - \delta$ we have:*

$$\mathcal{R}(\rho) \leq \hat{\mathcal{R}}(\rho) + \sqrt{\frac{\bar{D} \mathbb{E}_{\boldsymbol{\theta} \sim \pi} \mathbb{E}_{S \sim D^m} \left[(\mathcal{R}(\boldsymbol{\theta}) - \hat{\mathcal{R}}(\boldsymbol{\theta}))^2 \right]}{\delta}}, \quad (5)$$

where $\bar{D} = \chi^2(\rho||\pi) + 1$, $\mathcal{R}(\rho) = \mathbb{E}_{\theta \sim \rho}[\mathcal{R}(\theta)]$ and $\hat{\mathcal{R}}(\rho) = \mathbb{E}_{\theta \sim \rho}[\hat{\mathcal{R}}(\theta)]$.

The proof can be found in Appendix A.2. This bound gives a complexity that scales with the variance of the loss function, at the cost of a scaling factor $\frac{\bar{D}}{\delta}$. It can be thus used to directly derive a bound under a bounded loss-variance assumption, or— as we show later—when combined with the Poincaré assumption, to obtain a bound involving the input gradient $\|\nabla_{\mathbf{x}}\ell\|_2^2$.

3 PAC-Bayes bounds with input gradient-dependent complexity

Although the aforementioned bounds can be applied naively to each individual loss term in PIML and then combined via a union bound, doing so yields loose guarantees. First, minimising the bound for each loss independently typically produces different optimal values of λ , so $\sum_i \inf_{\lambda} g_i(\lambda) \geq \inf_{\lambda} \sum_i g_i(\lambda)$. Second, the union bound forces a sum of KL terms and also amplifies the penalty associated with the confidence parameter θ . To alleviate this looseness, we adopt a multi-task learning perspective introduced by [44]. Specifically, the PIML problem can be regarded as an extreme multi-task instance: all tasks share the same learnable architecture and differ only in fixed components used to compute each loss, with additional operators $\mathcal{D}, \mathcal{I}, \mathcal{B}$ forming the PDE/IC/BC residuals. Then, we can obtain substantially tighter bounds by treating the losses as a single composite risk and exploiting the following i.i.d. assumption over the collection of training sets.

Assumption 3.1 (i.i.d. sampling across tasks and closure under losses). *Let $\{S_i\}_{i=1}^{N_L}$ denote the collection of training datasets, where each dataset is given by $S_i = \{\mathbf{x}_{i,j}\}_{j=1}^{m_i}$. We assume that, for each $i \in \{1, \dots, N_L\}$, the samples $\{\mathbf{x}_{i,j}\}_{j=1}^{m_i}$ are drawn independently and identically distributed according to an underlying distribution D_i , i.e., $\mathbf{x}_{i,j} \stackrel{\text{i.i.d.}}{\sim} D_i$. Moreover, the datasets $\{S_i\}_{i=1}^{N_L}$ are mutually independent across tasks. Finally, for any measurable loss function ℓ_i applied independently to each sample $\mathbf{x}_{i,j}$, the transformed variables $\{\ell_i(\theta, \mathbf{x}_{i,j})\}_{j=1}^{m_i}$ remain i.i.d. within each task.*

Below we derive a generic sample-weighted PAC-Bayes-Chernoff bound for PIML.

Theorem 3.2. *Under Assumption 3.1, for any confidence level $\delta \in (0, 1)$, any prior $\pi \in \mathcal{M}(\Theta)$, for any posterior $\rho \in \mathcal{M}(\Theta)$, for any $\lambda > 0$, with probability at least $1 - \delta$ we have:*

$$\text{gen}^{\mathcal{S}}(\rho, S) \leq \inf_{\lambda} \left\{ \frac{\text{KL}(\rho||\pi) + \ln \frac{M}{\delta}}{\lambda(M-1)} + \frac{\sum_{i=1}^{N_L} m_i \mathbb{E}_{\rho}[\Lambda_{\theta}^{(i)}(\lambda)]}{M\lambda} \right\}. \quad (6)$$

The proof of Theorem 3.2 can be found in Appendix A.2. This result is central to our approach. Unlike standard PAC-Bayes analyses that treat each loss independently and combine guarantees via union bounds, Theorem 3.2 leverages the joint structure of PIML to control all tasks simultaneously. This leads to tighter bounds by avoiding both the duplication of complexity terms and suboptimal choices of tuning parameters across tasks. It holds for all $\lambda > 0$ and can be optimised over λ ; performing this optimisation incurs a $\ln M$ penalty that is applied jointly to all losses. Note that the complexity term obtained by applying a union bound to [6] is $\sum_{i=1}^{N_L} \inf_{\lambda} \left\{ \frac{\text{KL}(\rho||\pi) + \ln \frac{N_L m_i}{\delta}}{\lambda(M - \frac{1}{m_i})} + \frac{m_i \mathbb{E}_{\rho}[\Lambda_{\theta}^{(i)}(\lambda)]}{\lambda M} \right\}$. Even without invoking the sum of individual infima, this comparison already shows that our multi-task formulation leaves the KL term and the confidence term unamplified, thereby producing a strictly tighter bound. Theorem 3.2 will be used later on, to derive bounds for both PIML loss and gradient.

3.1 Bounds from Sobolev assumption

To make the above bound more intuitive, we need to control $\Lambda_{\theta}^{(i)}(\lambda)$ with a term that represents some properties of the target physical function such as its regularity (smoothness) in the input domain. Concretely, we assume that the underlying measure on the Sobolev space satisfies a Φ -Sobolev inequality [8], [4]. Specifically, for sufficiently smooth $f \in H^1(\Omega)$, the Φ -entropy of f is bounded by a constant multiple of $\|\nabla f\|_{L^2}^2$, thereby providing a flexible framework to capture different regimes of regularity and concentration. In our setting, this assumption acts as a smoothness condition on the function class, penalizing irregular behavior, enabling refined stability and concentration guarantees.

Assumption 3.3 (Sobolev-smoothness of the PIML model). *Let $\Omega \subset \mathbb{R}^{d_i}$ be a convex, bounded domain and let $\{D_i\}_{i=1}^{N_L}$ denote the underlying data distribution on Ω . We say that the PIML model*

class $u_{\theta}(\mathbf{x})$ satisfies the Sobolev-smoothness assumption for all θ if, for every loss term indexed by i , there exists $C_{S,i} > 0$ such that $\Lambda_{\theta}^{(i)}(\lambda) \leq \frac{C_{S,i}}{2} \lambda^2 \mathbb{E}_{\mathbf{x} \sim D} \left[\|\nabla_{\mathbf{x}} \ell_i(\theta, \mathbf{x})\|_2^2 \right]$.

Assumption 3.3 implies that the model $u_{\theta}(\mathbf{x})$ is sufficiently smooth so that both data loss and all physical residual losses also exhibit the smoothness in the sense of Φ -Sobolev inequality. It can be used to derive an oracle bound as shown in Lemma A.4 of Appendix A.3. We can make it empirical with the following assumption on the Lipschitz of the input-gradient of the losses.

Assumption 3.4 (Input-data Lipschitz). For any $\theta \in \Theta$, for any $\mathbf{x} \in \mathcal{X}$, and for all task i , we assume that the input-gradient is bounded, i.e., there exists $L_i > 0$ such that $\|\nabla_{\mathbf{x}} \ell_i(\theta, \mathbf{x})\|_2^2 \leq L_i$.

Assumption 3.4 is generally satisfied in standard PINNs under Sobolev smoothness. This is equivalent to say that the gradients are sub-gaussian, thus allowing us to control the CGF of the gradient norms. Then by making use of Theorem 3.2, we obtain the following empirical bound.

Theorem 3.5 (PAC-Bayes-Sobolev bound). Under Assumptions 3.1, 3.3 and 3.4, for any confidence level $\delta \in (0, 1)$, any prior $\pi \in \mathcal{M}(\Theta)$, for any posterior $\rho \in \mathcal{M}(\Theta)$, with probability at least $1 - \delta$ we have:

$$\text{gen}^S(\rho, S) \leq \frac{1}{M} \sqrt{2 \|\hat{\nabla}_{\text{PIML}_S}(\rho)\|_2^2 K(\rho, \pi, \delta) + L_{\text{PIML}_S} K(\rho, \pi, \delta)^{\frac{3}{2}}}, \quad (7)$$

where $\|\hat{\nabla}_{\text{PIML}_S}(\rho)\|_2^2 := \sum_{i=1}^{N_L} C_{S,i} \mathbb{E}_{\theta \sim \rho} \sum_{j=1}^{m_i} \left[\|\nabla_{\mathbf{x}} \ell_i(\theta, \mathbf{x}_{i,j})\|_2^2 \right]$; $K(\rho, \pi, \delta) := \frac{M(KL(\rho \|\pi) + \ln \frac{2M}{\delta})}{M-1}$ and $L_{\text{PIML}_S} := \sqrt{2 \sum_{i=1}^{N_L} m_i C_{S,i}^2 L_i^2}$.

The proof of Theorem 3.5 can be found in Appendix A.3. The bound in Theorem 3.5 exhibits a key structural property: the complexity term scales with the input-gradient norms of the losses. This reveals that smoother models, in the sense of smaller input gradients, enjoy tighter generalisation guarantees. In the PIML setting, this provides a formal explanation for the regularising effect of physical constraints, which implicitly enforce smoothness through differential operators. One part, the KL term $K(Q, P, \delta)$ favors posterior close to the prior, which can be efficiently learned while staying independent of posterior training data. The weighted gradient terms provide insights onto how input-gradient regularisation can help to reduce the generalisation gap.

3.2 Bounds from Poincaré assumption

In addition, and as a baseline counterpart to the Φ -Sobolev assumption, we can impose a *Poincaré inequality* as a direct link to the χ^2 -divergence bound in Theorem 2.1. It typically provides a weaker but fundamental form of regularity [13], [4]. For sufficiently smooth $f \in H^1(\Omega)$, this inequality controls the variance of f by its Dirichlet energy, link global fluctuations to the squared gradient norm, and can be directly plugged into the χ^2 -divergence bound in Theorem 2.1. Similarly to the previous section, it is natural to make the following smoothness assumption.

Assumption 3.6 (Poincaré-smoothness of the PIML model). Let $\Omega \subset \mathbb{R}^d$ be a convex, bounded domain and let $\{D_i\}_{i=1}^{N_L}$ denote the uniform probability measure on Ω . We say that the PIML model $u_{\theta}(\mathbf{x})$ satisfies the Poincaré-smoothness assumption if, for every loss term indexed by i , there exists $C_{P,i} > 0$ such that $\mathbb{V}_{\mathbf{x} \sim D}[\ell_i(\theta, \mathbf{x})] \leq C_{P,i} \mathbb{E}_{\mathbf{x} \sim D} \|\nabla \ell_i(\theta, \mathbf{x})\|_2^2$.

We now make use of this Poincaré-smoothness and Lipschitzness assumptions along with Theorem 2.1 and Theorem 3.2 to derive the following two empirical bounds corresponding to the two versions of generalisation gap presented in Section 2.1.

Theorem 3.7 (PAC-Bayes-Poincaré bounds). Under Assumptions 3.1, 3.6 and 3.4, for any confidence level $\delta \in (0, 1)$, any prior $\pi \in \mathcal{M}(\Theta)$, for any posterior $\rho \in \mathcal{M}(\Theta)$, for any $\lambda > 0$, with probability at least $1 - \delta$ we have:

$$\text{gen}(\rho, S) \leq \sqrt{\frac{(2 \|\hat{\nabla}_{\text{PIML}_P}(\pi)\|_2^2 + L_{\text{PIML}_P} K(\delta)^{\frac{1}{2}}) \bar{D}}{\delta}}, \quad (8)$$

$$\text{gen}^S(\rho, S) \leq \frac{1}{M} \sqrt{\frac{(2 \|\hat{\nabla}_{\text{PIML}_P}^S(\pi)\|_2^2 + L_{\text{PIML}_P}^S K(\delta)^{\frac{1}{2}}) \bar{D}}{\delta}}, \quad (9)$$

$$\begin{aligned}
\text{where } \|\hat{\nabla}_{\text{PIMLP}}(\pi)\|_2^2 &:= \sum_{i=1}^{N_L} \frac{C_{P,i}}{m_i^2} \mathbb{E}_{\theta \sim \pi} \sum_{j=1}^{m_i} \|\nabla \ell_i(\theta, \mathbf{x}_{i,j})\|_2^2; \quad \|\hat{\nabla}_{\text{PIMLP}}^S(\pi)\|_2^2 := \\
\sum_{i=1}^{N_L} C_{P,i} \mathbb{E}_{\theta \sim \pi} \sum_{j=1}^{m_i} \|\nabla \ell_i(\theta, \mathbf{x}_{i,j})\|_2^2; \quad L_{\text{PIMLP}} &:= \sqrt{2 \sum_{i=1}^{N_L} \frac{C_{P,i}^2 L_i^2}{m_i^3}}; \quad L_{\text{PIMLP}}^S := \\
\sqrt{2 \sum_{i=1}^{N_L} m_i C_{P,i}^2 L_i^2}; \text{ and } K(\delta) &:= \frac{M \ln \frac{2M}{\delta}}{M-1}.
\end{aligned}$$

The proof of this theorem can be found in Appendix A.4. We can see that the complexity of these bounds contains a similar structure with the Sobolev-based bound in Theorem 3.5. However, the multiplicative term is now scaled by an expected weighted sum of the input gradients under the prior distribution. It is obvious that the two Poincaré bounds here are less tighter than the Sobolev counterpart: the confidence penalty scales as $\frac{1}{\delta}$ in the former versus $\ln(\frac{1}{\delta})$ in the latter, and the $\chi^2 + 1$ term grows much faster (e.g., exponentially in the case of Gaussian distribution). As a result, Poincaré bounds are less flexible from an optimisation perspective.

4 Experimental evaluation on physics-informed neural networks

In this section, we present how to concretise the bounds in the previous section from a practical point of view, by first estimating the constants $\{C_{S,i}, C_{P,i}, L_i\}$ from Assumptions 3.3, 3.6 and 3.4.

4.1 Refining the assumptions with localisation and clipping

Tighter bounds require finite constants that make the proposed inequalities hold uniformly over the hypothesis class. Empirical observations (Appendix B.2) show that, when sampling models at increasing distance R from a well-trained model, the input-gradient of the losses—in particular the PDE and data-fidelity terms—grow rapidly, exceeding 10^8 already at $R = 1$. This explosive growth is highly detrimental to the bounds’ tightness and substantially impairs the posterior’s ability to learn.

However, once training has relatively converged, models typically operate in a region where all loss components remain small and exhibit limited variability. We empirically observe that the losses are much smaller than 100, and if we apply a clipping at that value, it almost surely has no impact to the loss value. Nevertheless, such clipping is highly beneficial when estimating those constants, as it ensures that the losses remain locally bounded in the neighborhood of a well-trained model, which in turn bounds their variances and stabilises the associated CGF. As a consequence, we can also clip input-gradients while still being able to find constants satisfying the Sobolev and Poincaré assumptions. To avoid unnecessary loose bounds, we select L_i by balancing its trade-off with the Poincaré and Sobolev constants, exploiting their asymptotic proportionality to restrict the search to $C_{P,i}$ and L_i . We first select candidate pairs minimizing $C_{P,i} L_i$ and then chooses the one with the smallest $C_{P,i}$, while estimating constants within a radius R around the prior. The radius is chosen to ensure sampled models remain close to the prior. In practice $R^2 \sim (3\sigma)^2 d_\theta$ suffices to ensure that, with d_θ being the number of learnable parameters of model. Finally, observe that choosing a sufficiently large clipping threshold leaves the loss values unchanged, while the bounds with clipped values are naturally upper-bounded by their unclipped counterparts. Consequently, the bounds stated in Theorems 3.5 and 3.7 remain valid when the associated constants are estimated using the above scheme. For improved training behavior and interpretability, we therefore employ the unclipped bounds during both training and evaluation. Further details are deferred to Appendix B.3.

4.2 Self-bounding-aware algorithm

The optimisation of the presented bounds is presented in Algorithm 1. It consists of two main steps: **1)** learning a prior π from prior training sets then estimating the constants from the calibration set; and **2)** learning the posterior ρ to minimise the bounds via their respective stochastic surrogates.

Step 1. The prior model’s parameters θ_π is obtained after N_T iterations using a mini-batch gradient descent algorithm. For each iteration, we randomly sample a set of mini-batches from the set of prior datasets S_{prior} and update θ_π by minimising the adaptively weighted risk $\hat{\mathcal{R}}_{\text{PIMLP}}(\theta)$. To ensure θ_π achieves good performance, we use the neural tangent kernel (NTK) training scheme [41]. From this learned prior θ_π , we search for the constants of Sobolev, Poincaré and Lipschitz assumptions (Lines 6-11 of Algorithm 1). We begin by clipping all losses at 100, then using a calibration dataset S_{calib} to search for the clipping threshold L_i favoring small bounds.

Step 2. Given the learned prior $\pi = \mathcal{N}(\boldsymbol{\theta}_\pi, \sigma^2 \mathbf{1}_{d_\theta})$ and the set of estimated constants $\{(C_{S,i}, C_{P,i}, L_i)\}_{i=1}^{N_L}$, we initialise the posterior parameter $\boldsymbol{\theta}_\rho$ from $\boldsymbol{\theta}_\pi$ and optimise it during $N_{T'}$ iterations. For each iteration, we randomly draw a set of mini-batches from S_{post} , and sample $\boldsymbol{\theta}' := \boldsymbol{\theta}_\rho + \epsilon$ with $\epsilon \sim \mathcal{N}(\mathbf{0}, \sigma^2 \mathbf{1}_{d_\theta})$. Note that in a balanced setting (i.e., $m_i = m, \forall i$), the sample-centric bounds can be rewritten as an equally-weighted bound and we can thus learn to directly minimise the bound (**self-bounding**). Otherwise, in a more general scenario where we have diverse sample sizes, there is no guarantee that reducing the bound $\mathcal{U}^S(\rho)$ on $\mathcal{R}_{\text{PIML}}^S(\rho)$ will also reduce the bound on the target true risk $\mathcal{R}_{\text{PIML}}(\rho)$. To alleviate this issue, we can simply learn to minimise the following union-bounds to directly control the true risk of each loss (**bounding-aware**):

$$\sum_{i=1}^{N_L} \left\{ \hat{\mathcal{R}}_i(\boldsymbol{\theta}') + \sqrt{2 \frac{C_{S,i}}{m_i} \sum_{j=1}^{m_i} \left[\|\nabla_{\mathbf{x}} \ell_i(\boldsymbol{\theta}', \mathbf{x}_{i,j})\|_2^2 \right] K_i(\boldsymbol{\theta}_\rho) + \sqrt{2} L_i C_{S,i} K_i(\boldsymbol{\theta}_\rho)^{\frac{3}{2}}} \right\}, \quad (10)$$

$$\sum_{i=1}^{N_L} \left\{ \hat{\mathcal{R}}_i(\boldsymbol{\theta}') + \sqrt{\frac{N_L}{\delta} \left(2 \frac{C_{P,i}}{m_i^2} \sum_{j=1}^{m_i} \|\nabla \ell_i(\pi, \mathbf{x}_{i,j})\|_2^2 + \sqrt{2} \frac{L_i C_{P,i}}{m_i} K_i(\boldsymbol{\theta}_\pi)^{\frac{1}{2}} \right) \exp\left(\frac{r^2(\boldsymbol{\theta}_\rho)}{\sigma^2}\right)} \right\}, \quad (11)$$

where $\|\nabla \ell_i(\pi, \mathbf{x}_{i,j})\|_2^2 := \mathbb{E}_{\boldsymbol{\theta} \sim \pi} \|\nabla \ell_i(\boldsymbol{\theta}, \mathbf{x}_{i,j})\|_2^2$, $r^2(\boldsymbol{\theta}) := \|\boldsymbol{\theta} - \boldsymbol{\theta}_\pi\|_2^2$ and $K_i(\boldsymbol{\theta}) := \frac{1}{m_i - 1} \left(\frac{r^2(\boldsymbol{\theta})}{2\sigma^2} + \ln \frac{2N_L m_i}{\delta} \right)$. After learning, we can obtain the final bound $\mathcal{U}(\rho)$ by solving an optimisation problem (Step 2, Line 8 of Algorithm 1) with the linear constraint offered by the bounds in Equation 7 or 9. See Appendix B.4 for more details.

Algorithm 1 Optimisation of the physics-informed PAC-Bayes bounds

Require: Prior datasets S_{prior} ; Calibration datasets S_{calib} ; posterior datasets S_{post} , initial parameters $\boldsymbol{\theta}_0 \in \mathbb{R}^{d_\theta}$; Predefined variance parameter σ ; number of iterations N_T and $N_{T'}$; number of preselected clipping values k ; number of draws per search N_{draw} .

Step 1 - prior learning & constant estimation

1. $\boldsymbol{\theta}_\pi \leftarrow \boldsymbol{\theta}_0$
2. **for** $t = 1$ to N_T **do**
3. Draw a set of mini-batches from S_{prior}
4. $\boldsymbol{\theta}_\pi \leftarrow$ Update $\boldsymbol{\theta}_\pi$ with $\hat{\mathcal{R}}_{\text{PIML}_\lambda}(\boldsymbol{\theta}_\pi)$
5. **end for**
6. **for** loss $i = 1$ to N_L **do**
7. $\mathcal{S}_\tau \leftarrow \{C_p(\tau, 1, N_{draw}) \mid \tau \in \mathcal{T}\}$
8. $\mathcal{L} \leftarrow$ Smallest $_k(\mathcal{S}_\tau)$
9. $L_i \leftarrow \arg \min_{\tau \in \mathcal{L}} C_p(\tau, 1, N_{draw})$
10. Select $C_{P,i}, C_{S,i}$ from clipped gradient norm of loss i at L_i
11. **end for**

Step 2 - bound minimisation

1. $\boldsymbol{\theta}_\rho \leftarrow \boldsymbol{\theta}_\pi$
 2. **for** $t = 1$ to $N_{T'}$ **do**
 3. Draw a set of mini-batches from S_{post}
 4. Sample a noise $\epsilon \sim \mathcal{N}(\mathbf{0}, \sigma^2 \mathbf{1}_{d_\theta})$
 5. $\boldsymbol{\theta}' \leftarrow \boldsymbol{\theta}_\rho + \epsilon$
 6. $\boldsymbol{\theta}_\rho \leftarrow$ Update $\boldsymbol{\theta}_\rho$ with either direct surrogates (**self-bounding**); or 10 or 11 (**bounding-aware**)
 7. **end for**
 8. (Optional) Compute $\mathcal{U}^S(\rho)$ then solve the optimisation problem to obtain $\mathcal{U}(\rho)$
 9. **return** $\boldsymbol{\theta}_\rho, \mathcal{U}(\rho)$
-

4.3 Experiments

In this section, we empirically illustrate that our PAC-Bayesian framework, with Algorithm 1 above, is able to provide generalisation guarantees with non-vacuous bounds for the PIML risk.

Benchmark. For a comprehensive evaluation, we consider three benchmark problems: 1D-Reaction, 1D-Wave, and Convection. For each physical loss, we split the samples into three disjoint sets: 10k prior, 30k posterior, and 20k calibration points. Beyond a baseline with 30k posterior samples and 10k calibration points from observational data, we also study a limited-data regime with only 300 (and as few as 2) observations to reflect practical data scarcity. In these restricted cases, we use all of these samples to train the posterior, while employing the constants of the initial loss ℓ_{ic} for the loss ℓ_d (as they are both approximation errors). **Note that the prior model is trained using only the physics-based loss terms in all settings.** See Appendix B.5 for more details on implementation.

Bounds. We denote the bound obtained via Theorem 3.5 as **Ours-Sob**. For Theorem 2, the bound using Inequality 8 is denoted **Ours-Poi.**, while the sample-weighted version based on Inequality 9 is

written as **Ours-Poi._g**. To our knowledge, no generalisation bounds incorporating priors exist for PIML; thus we propose to compare ourselves with baseline approaches under the same assumptions. In particular, **U-Sob.** denotes the union bound over individual losses using the Sobolev bound (inspired by [6]), and **U-Poi.** analogously denotes the union of Poincaré bounds.

Table 1: Empirical test risk/ generalisation bounds on 1D-Wave with different observation data sample sizes. Here $\ell_d \sim 1e-4$ which is very small compared to the total risk $\hat{\mathcal{R}}_{\text{test}}(\rho)$.

Bound	Ours-Sob.	Ours-Poi.	Ours-Poi. _g	U-Sob.	U-Poi.
$m_d = 3e4$	4.22e-1/ 6.76 e-1	4.41e-1/7.32e-1	4.41e-1/7.32e-1	4.25e-1/6.80e-1	4.47e-1/1.12
$m_d = 300$	4.23e-1/ 7.01 e-1	4.39e-1/7.58e-1	4.46e-1/1.02e-1	4.23e-1/7.08e-1	4.46e-1/1.43
$m_d = 2$	4.45e-1/ 1.75	4.49e-1/2.02	4.50e-1/4.19	4.45e-1/1.76	4.50e-1/4.12

Results. In our experiment, we first evaluate numerically the bounds above in a vanilla setting, where we have equal sample size by setting $m_d = 3 \times 10^4$. Figure 1 shows that our bounds provide tighter guarantees than the union-based counterparts, i.e., , under $2 \times$ of the test risks in all cases. It is also shown that Sobolev-based bounds (**Ours-Sob** and **U-Sob.**) are better than Poincaré-based counterparts, with **Ours-Sob** achieves smallest values in all problems. Figure 2 then depicts the results in a more restricted case where we only have $m_d = 300$ observational points. While the bounds on 1D-Wave only increase slightly, the effects on 1D-Reaction and Convection are more significant, with the ratio $\mathcal{U}(\rho)/\hat{\mathcal{R}}_{\text{test}}(\rho) \sim 10$. This arises from overly pessimistic constants when employing constants of ℓ_{ic} for ℓ_d in one part, and from the significantly larger gradients (less regularity and greater difficulty) exhibited by ℓ_d in the other. Besides, Table 1 shows that if the model learns well and achieves low ℓ_d (also small $\|\nabla_{\mathbf{x}} \ell_d(\boldsymbol{\theta}, \mathbf{x})\|_2^2$), it is possible to achieve tight bounds with only a few samples of observational data. Additional results and baseline are available in Appendix B.6.

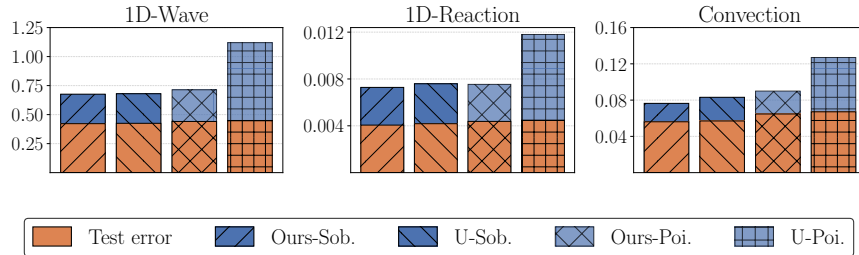


Figure 1: Test error and generalisation bounds when $m_d = 30k$.

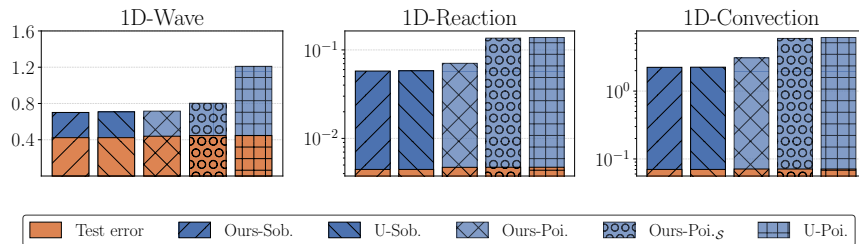


Figure 2: Test error and generalisation bounds when $m_d = 300$.

5 Conclusion

We introduced a PAC-Bayesian framework for physics-informed machine learning that provides generalisation guarantees in regression settings with unbounded losses. By adopting a multi-task perspective, we derived bounds that jointly control data and physics objectives, avoiding the looseness

of standard union-bound approaches. Our analysis reveals that the generalisation gap is governed by input-gradient dependent complexity terms, establishing a direct connection between physical regularity and statistical performance. We discuss the limitations of our work in Appendix C.

Beyond the theoretical contributions, we proposed a self-bounding-aware learning algorithm and a practical procedure to estimate the required constants, enabling the optimisation of generalisation bounds in realistic settings. Empirical results on standard PDE benchmarks demonstrate that our bounds are non-vacuous and can be effectively minimised during training.

As far as we know, this paper is the first PAC-Bayesian framework for PIML, accompanied with an effective algorithm able to optimise the proposed bounds. Overall, this work provides a principled statistical foundation for physics-informed learning and opens several directions for future research, including tighter data-dependent analyses, constructions of physics-informed priors, extensions to more complex physical systems, and connections with implicit regularisation in deep learning.

References

- [1] Pierre Alquier. User-friendly introduction to PAC-Bayes bounds. *Foundations and Trends in Machine Learning*, 17(2):174–303, 01 2024.
- [2] Pierre Alquier and Benjamin Guedj. Simpler PAC-Bayesian bounds for hostile data. *Machine Learning*, 107(5), 2018.
- [3] Pierre Alquier, James Ridgway, and Nicolas Chopin. On the properties of variational approximations of Gibbs posteriors. *Journal of Machine Learning Research*, 17(236):1–41, 2016.
- [4] Dominique Bakry, Ivan Gentil, and Michel Ledoux. *Analysis and Geometry of Markov Diffusion Operators*. Springer, 2014.
- [5] Luc Bégin, Pascal Germain, François Laviolette, and Jean-François Roy. PAC-Bayesian bounds based on the rényi divergence. In *Proceedings of the 19th International Conference on Artificial Intelligence and Statistics*, volume 51 of *Proceedings of Machine Learning Research*, pages 435–444, Cadiz, Spain, 09–11 May 2016. PMLR.
- [6] Ioar Casado, Luis A. Ortega, Aritz Pérez, and Andres R Masegosa. PAC-Bayes-Chernoff bounds for unbounded losses. In *The Thirty-eighth Annual Conference on Neural Information Processing Systems*, 2024.
- [7] Olivier Catoni. *Statistical learning theory and stochastic optimization. Ecole d’été de probabilités de Saint-Flour XXXI-2001*. Springer, 2004. Collection : Lecture notes in mathematics n°1851.
- [8] Djalil Chafaï. Entropies, convexity, and functional inequalities: on ϕ -entropies and ϕ -Sobolev inequalities. *Journal of Mathematics of Kyoto University*, 44, 08 2004.
- [9] Monroe David Donsker and Sathamangalam Ranga Srinivasa Varadhan. Asymptotic evaluation of certain Markov process expectations for large time, I. *Communications on Pure and Applied Mathematics*, 28(1):1–47, 1975.
- [10] Nathan Doumèche, Francis Bach, Gérard Biau, and Claire Boyer. Physics-informed machine learning as a kernel method. In *The Thirty Seventh Annual Conference on Learning Theory, June 30 - July 3, 2023, Edmonton, Canada*, Proceedings of Machine Learning Research, pages 1399–1450. PMLR, 2024.
- [11] Nathan Doumèche, Francis Bach, Gérard Biau, and Claire Boyer. Physics-informed kernel learning. *J. Mach. Learn. Res.*, 26:124:1–124:39, 2025.
- [12] Nathan Doumèche, Gérard Biau, and Claire Boyer. On the convergence of PINNs. *Bernoulli*, 31(3):2127–2151, 2025.
- [13] Lawrence Craig Evans. *Partial Differential Equations*. American Mathematical Society, 2 edition, 2010.

- [14] Itai Gat, Yossi Adi, Alex Schwing, and Tamir Hazan. On the importance of gradient norm in PAC-bayesian bounds. In *Annual Conference on Neural Information Processing Systems*, 2022.
- [15] Pascal Germain, Francis Bach, Alexandre Lacoste, and Simon Lacoste-Julien. PAC-Bayesian theory meets bayesian inference. In *Advances in Neural Information Processing Systems*, volume 29. Curran Associates, Inc., 2016.
- [16] Pascal Germain, Alexandre Lacasse, Mario Marchand, Sara Shanian, and François Laviolette. From pac-bayes bounds to kl regularization. In Y. Bengio, D. Schuurmans, J. Lafferty, C. Williams, and A. Culotta, editors, *Advances in Neural Information Processing Systems*, volume 22. Curran Associates, Inc., 2009.
- [17] Benjamin Guedj. A primer on PAC-Bayesian learning. In *Proceedings of the second congress of the French Mathematical Society*, volume 33, 2019.
- [18] Ruixin Guo, Ruoming Jin, Xinyu Li, and Yang Zhou. PAC-Bayes bounds for multivariate linear regression and linear autoencoders. In *The Thirty-ninth Annual Conference on Neural Information Processing Systems*, 2025.
- [19] Maxime Haddouche and Benjamin Guedj. PAC-Bayes generalisation bounds for heavy-tailed losses through supermartingales. *Transactions on Machine Learning Research*, 2023.
- [20] Maxime Haddouche, Benjamin Guedj, Omar Rivasplata, and John Shawe-Taylor. PAC-Bayes unleashed: Generalisation bounds with unbounded losses. *Entropy*, 23(10), 2021.
- [21] Maxime Haddouche, Paul Viillard, Umut Şimşekli, and Benjamin Guedj. A PAC-Bayesian Link Between Generalisation and Flat Minima. In *ALT 2025 - 36th International Conference on Algorithmic Learning Theory*, pages 1–31, Milan, Italy, February 2025.
- [22] Fredrik Hellström, Giuseppe Durisi, Benjamin Guedj, and Maxim Raginsky. *Generalization Bounds: Perspectives from Information Theory and PAC-Bayes*. Foundations and Trends in Machine Learning, 2025.
- [23] Matthew Holland. PAC-Bayes under potentially heavy tails. In *Advances in Neural Information Processing Systems*, volume 32. Curran Associates, Inc., 2019.
- [24] Yuling Jiao, Yanming Lai, Dingwei Li, Xiliang Lu, Fengru Wang, Yang Wang, and Jerry Zhijian Yang. A rate of convergence of physics informed neural networks for the linear second order elliptic PDEs. *Communications in Computational Physics*, 31(4):1272–1295, 2022.
- [25] George Em Karniadakis, Ioannis G. Kevrekidis, Lu Lu, Paris Perdikaris, Sifan Wang, and Liu Yang. Physics-informed machine learning. *Nature Reviews Physics*, 3(6), 5 2021.
- [26] Yiping Lu, Haoxuan Chen, Jianfeng Lu, Lexing Ying, and Jose H. Blanchet. Machine learning for elliptic PDEs: Fast rate generalization bound, neural scaling law and minimax optimality. In *The Tenth International Conference on Learning Representations, ICLR 2022, Virtual Event, April 25-29, 2022*, 2022.
- [27] Levi McClenny and Ulisses Braga-Neto. Self-adaptive physics-informed neural networks using a soft attention mechanism. *J. Comput. Phys.*, 474:111722, 2020.
- [28] Siddhartha Mishra and Roberto Molinaro. Estimates on the generalization error of physics-informed neural networks for approximating a class of inverse problems for PDEs. *IMA Journal of Numerical Analysis*, 42(2):981–1022, 04 2022.
- [29] Yuki Ohnishi and Jean Honorio. Novel change of measure inequalities with applications to PAC-Bayesian bounds and monte carlo estimation. In *Proceedings of The 24th International Conference on Artificial Intelligence and Statistics*, volume 130 of *Proceedings of Machine Learning Research*, pages 1711–1719. PMLR, 13–15 Apr 2021.
- [30] Adam Paszke, Sam Gross, Francisco Massa, Adam Lerer, James Bradbury, Gregory Chanan, Trevor Killeen, Zeming Lin, Natalia Gimelshein, Luca Antiga, Alban Desmaison, Andreas Kopf, Edward Z. Yang, Zachary DeVito, Martin Raison, Alykhan Tejani, Sasank Chilamkurthy, Benoit Steiner, Lu Fang, Junjie Bai, and Soumith Chintala. Pytorch: An imperative style, high-performance deep learning library. In *Advances in Neural Information Processing Systems* 32, pages 8024–8035. Curran Associates, Inc., 2019.

- [31] Antoine Picard-Weibel and Benjamin Guedj. On change of measure inequalities for f-divergences. *ArXiv*, abs/2202.05568, 2022.
- [32] Maziar Raissi, Paris Perdikaris, and George E Karniadakis. Physics-informed neural networks: A deep learning framework for solving forward and inverse problems involving nonlinear partial differential equations. *Journal of Computational physics*, 2019.
- [33] Borja Rodríguez-Gálvez, Ragnar Thobaben, and Mikael Skoglund. More PAC-Bayes bounds: From bounded losses, to losses with general tail behaviors, to anytime validity. *Journal of Machine Learning Research*, 25(110):1–43, 2024.
- [34] Sergio Rojas, Paweł Maczuga, Judit Muñoz-Matute, David Pardo, and Maciej Paszyński. Robust variational physics-informed neural networks. *Computer Methods in Applied Mechanics and Engineering*, 425:116904, 2024.
- [35] Tim De Ryck and Siddhartha Mishra. Generic bounds on the approximation error for physics-informed (and) operator learning. In *Annual Conference on Neural Information Processing Systems*, 2022.
- [36] Anna Scampicchio, Leonardo Felipe Toso, Rahel Rickenbach, James Anderson, and Melanie Zeilinger. Physics-informed learning under mixing: How physical knowledge speeds up learning. In *The Fourteenth International Conference on Learning Representations*, 2026.
- [37] Vera Shalaeva, Alireza Fakhrizadeh Esfahani, Pascal Germain, and Mihály Petreczky. Improved PAC-Bayesian bounds for linear regression. In *AAAI Conference on Artificial Intelligence*, 2019.
- [38] Yeonjong Shin, Zhongqiang Zhang, and George Em Karniadakis. Error estimates of residual minimization using neural networks for linear PDEs. *Journal of Machine Learning for Modeling and Computing*, 4(4), 2023.
- [39] Makoto Takamoto, Timothy Praditia, Raphael Leiteritz, Daniel MacKinlay, Francesco Alesiani, Dirk Pflüger, and Mathias Niepert. PDEBENCH: An Extensive Benchmark for Scientific Machine Learning. In *Advances in Neural Information Processing Systems*, volume 35, pages 1596–1611. Curran Associates, Inc., 2022.
- [40] Paul Viallard, Maxime Haddouche, Umut Şimşekli, and Benjamin Guedj. Learning via Wasserstein-based high probability generalisation bounds. In *Annual Conference on Neural Information Processing Systems (NeurIPS)*, 2023.
- [41] Sifan Wang, Xinling Yu, and Paris Perdikaris. When and why PINNs fail to train: A neural tangent kernel perspective. *Journal of Computational Physics*, 449:110768, 2022.
- [42] Xianliang Xu, Ye Li, and Zhongyi Huang. Refined generalization analysis of the deep Ritz method and physics-informed neural networks. In *Proceeding of the International Conference on Machine Learning (ICML)*, 2025.
- [43] Hossein Zakerinia, Amin Behjati, and Christoph Lampert. More flexible PAC-Bayesian meta-learning by learning learning algorithms. In *Proceedings of the 41st International Conference on Machine Learning*, volume 235 of *Proceedings of Machine Learning Research*, pages 58122–58139. PMLR, 21–27 Jul 2024.
- [44] Hossein Zakerinia and Christoph Lampert. Fast rate bounds for multi-task and meta-learning with different sample sizes. In *The Thirty-ninth Annual Conference on Neural Information Processing Systems*, 2025.

A Proofs

A.1 Auxiliary lemmas

Lemma A.1 (General PAC-Bayesian Bound). *For any distribution D on \mathcal{X} , for any hypothesis set Θ , for any prior $\pi \in \mathcal{M}(\Theta)$, for any measurable function $\varphi : \Theta \times \mathcal{X}^m \rightarrow \mathbb{R}$, for any posterior $\rho \in \mathcal{M}(\Theta)$ we have:*

$$\mathbb{P}_{S \sim D^m} \left[\mathbb{E}_{\boldsymbol{\theta} \sim \rho} \varphi(\boldsymbol{\theta}, S) \leq \text{KL}(\rho \| \pi) + \ln \left(\frac{1}{\delta} \mathbb{E}_{S' \sim D^m} \mathbb{E}_{\boldsymbol{\theta}' \sim \pi} e^{\varphi(\boldsymbol{\theta}', S')} \right) \right] \geq 1 - \delta. \quad (12)$$

Proof. Applying Donsker-Varadhan variational formula [9] we obtain

$$\mathbb{E}_{\boldsymbol{\theta} \sim \rho} \varphi(\boldsymbol{\theta}, S) \leq \text{KL}(\rho \| \pi) + \ln \left[\mathbb{E}_{\boldsymbol{\theta}' \sim \pi} \left(e^{\varphi(\boldsymbol{\theta}', S)} \right) \right]. \quad (13)$$

Now applying Markov's inequality to the exponential term, we have:

$$\begin{aligned} \mathbb{P}_{S \sim D^m} \left[\mathbb{E}_{\boldsymbol{\theta}' \sim \pi} \left(e^{\varphi(\boldsymbol{\theta}', S)} \right) \leq \frac{1}{\delta} \mathbb{E}_{S' \sim D^m} \mathbb{E}_{\boldsymbol{\theta}' \sim \pi} e^{\varphi(\boldsymbol{\theta}', S')} \right] &\geq 1 - \delta \\ \Leftrightarrow \mathbb{P}_{S \sim D^m} \left[\ln \left(\mathbb{E}_{\boldsymbol{\theta}' \sim \pi} \left(e^{\varphi(\boldsymbol{\theta}', S)} \right) \right) \leq \ln \left(\frac{1}{\delta} \mathbb{E}_{S' \sim D^m} \mathbb{E}_{\boldsymbol{\theta}' \sim \pi} e^{\varphi(\boldsymbol{\theta}', S')} \right) \right] &\geq 1 - \delta. \end{aligned} \quad (14)$$

Combining 14 with 13, we complete the proof. \square

Lemma A.2 ([29], Lemma 9). *For any prior $\pi \in \mathcal{M}(\Theta)$, for any measurable function $\varphi : \Theta \times \mathcal{X}^m \rightarrow \mathbb{R}$, for any posterior $\rho \in \mathcal{M}(\Theta)$ we have*

$$\mathbb{E}_{\boldsymbol{\theta} \sim \rho} [\varphi] \leq \sqrt{(\chi^2(\rho \| \pi) + 1) \mathbb{E}_{\boldsymbol{\theta} \sim \pi} [\varphi^2]} \quad (15)$$

Proposition A.3 (Multi-task Cramér-Chernoff). *Define the sample-weighted cumulant generating function (CGF) as $\Lambda_{\boldsymbol{\theta}}^S(\lambda) = \frac{1}{M} \sum_{i=1}^{N_L} m_i \Lambda_{\boldsymbol{\theta}}(\lambda)$. For any $\boldsymbol{\theta} \in \Theta$ and $a \in \mathbb{R}$,*

$$\mathbb{P}_S [\text{gen}^S(\boldsymbol{\theta}, S) \geq a] \leq e^{-M \Lambda_{\boldsymbol{\theta}}^{S*}(a)} \quad (16)$$

where $\Lambda_{\boldsymbol{\theta}}^{S*}(a) = \sup_{\lambda} \{\lambda a - \Lambda_{\boldsymbol{\theta}}^S(\lambda)\}$ is the Cramér transform of the sample-centric CGF above.

Proof. Applying Markov's inequality and using Assumption 3.1, we have that

$$\begin{aligned} \mathbb{P}_S [\text{gen}^S(\boldsymbol{\theta}, S) \geq a] &= \mathbb{P}_S \left[e^{M \lambda \text{gen}^S(\boldsymbol{\theta}, S)} \geq e^{M \lambda a} \right] \\ &\leq e^{-M \lambda a} \mathbb{E}_S \left[e^{M \lambda \text{gen}^S(\boldsymbol{\theta}, S)} \right] \\ &= e^{-M \lambda a} \mathbb{E}_S \left[\exp \left(\lambda \sum_{i=1}^{N_L} \sum_{j=1}^{m_i} (\mathcal{R}_i(\boldsymbol{\theta}) - \ell_i(\boldsymbol{\theta}, \mathbf{x}_{i,j})) \right) \right] \\ &= e^{-M \lambda a} \mathbb{E}_S \left[\prod_{i=1}^{N_L} \prod_{j=1}^{m_i} \exp(\lambda (\mathcal{R}_i(\boldsymbol{\theta}) - \ell_i(\boldsymbol{\theta}, \mathbf{x}_{i,j}))) \right] \\ &= e^{-M \lambda a} \left[\prod_{i=1}^{N_L} \prod_{j=1}^{m_i} \mathbb{E}_{x_{i,j} \sim \mathcal{D}_i} \exp(\lambda (\mathcal{R}_i(\boldsymbol{\theta}) - \ell_i(\boldsymbol{\theta}, \mathbf{x}_{i,j}))) \right] \\ &= e^{-M \lambda a} \left[\prod_{i=1}^{N_L} \prod_{j=1}^{m_i} e^{\Lambda_{\boldsymbol{\theta}}^{(i)}(\lambda)} \right] = e^{-M \lambda a} e^{\sum_{i=1}^{N_L} m_i \Lambda_{\boldsymbol{\theta}}^{(i)}(\lambda)} \\ &= e^{-M(\lambda a - \Lambda_{\boldsymbol{\theta}}^S(\lambda))}. \end{aligned}$$

Since this holds $\forall \lambda > 0$, we have that

$$\begin{aligned} \mathbb{P}_S \left[\text{gen}^S(\boldsymbol{\theta}, S) \geq a \right] &\leq \inf_{\lambda} e^{-M(\lambda a - \Lambda_{\boldsymbol{\theta}}^S(\lambda))} \\ &= e^{-M \sup_{\lambda} (\lambda a - \Lambda_{\boldsymbol{\theta}}^S(\lambda))} = e^{-M \Lambda_{\boldsymbol{\theta}}^{S^*}(a)}, \end{aligned}$$

where the last equality comes from the definition. This completes the proof. \square

A.2 Proofs of oracle bounds

Theorem 2.1 (Generalised from Ohnisi and Honorio [29]). *For any confidence level $\delta \in (0, 1)$, any prior $\pi \in \mathcal{M}(\Theta)$, for any posterior $\rho \in \mathcal{M}(\Theta)$, with probability at least $1 - \delta$ we have:*

$$\mathcal{R}(\rho) \leq \hat{\mathcal{R}}(\rho) + \sqrt{\frac{\bar{D} \mathbb{E}_{\boldsymbol{\theta} \sim \pi} \mathbb{E}_{S \sim D^m} \left[(\mathcal{R}(\boldsymbol{\theta}) - \hat{\mathcal{R}}(\boldsymbol{\theta}))^2 \right]}{\delta}}, \quad (5)$$

where $\bar{D} = \chi^2(\rho \parallel \pi) + 1$, $\mathcal{R}(\rho) = \mathbb{E}_{\boldsymbol{\theta} \sim \rho} [\mathcal{R}(\boldsymbol{\theta})]$ and $\hat{\mathcal{R}}(\rho) = \mathbb{E}_{\boldsymbol{\theta} \sim \rho} [\hat{\mathcal{R}}(\boldsymbol{\theta})]$.

Proof. Applying Lemma A.2 with $\varphi = |\mathcal{R}(\boldsymbol{\theta}) - \hat{\mathcal{R}}(\boldsymbol{\theta})|$, then combining with Jensen's inequality we have that

$$\left| \mathbb{E}_{\boldsymbol{\theta} \sim \rho} [\mathcal{R}(\boldsymbol{\theta})] - \mathbb{E}_{\boldsymbol{\theta} \sim \rho} [\hat{\mathcal{R}}(\boldsymbol{\theta})] \right| \leq \mathbb{E}_{\boldsymbol{\theta} \sim \rho} |\mathcal{R}(\boldsymbol{\theta}) - \hat{\mathcal{R}}(\boldsymbol{\theta})| \leq \sqrt{\bar{D} \mathbb{E}_{\boldsymbol{\theta} \sim \pi} [(\mathcal{R}(\boldsymbol{\theta}) - \hat{\mathcal{R}}(\boldsymbol{\theta}))^2]} \quad (17)$$

Now using Markov inequality and Fubini's theorem, we have that

$$\begin{aligned} \mathbb{P}_{S \sim D^m} \left[\mathbb{E}_{\boldsymbol{\theta} \sim \pi} [(\mathcal{R}(\boldsymbol{\theta}) - \hat{\mathcal{R}}(\boldsymbol{\theta}))^2] \geq \epsilon \right] &\leq \frac{1}{\epsilon} \mathbb{E}_{S \sim D^m} \mathbb{E}_{\boldsymbol{\theta} \sim \pi} [(\mathcal{R}(\boldsymbol{\theta}) - \hat{\mathcal{R}}(\boldsymbol{\theta}))^2] \\ &= \frac{1}{\epsilon} \mathbb{E}_{\boldsymbol{\theta} \sim \pi} \mathbb{E}_{S \sim D^m} [(\mathcal{R}(\boldsymbol{\theta}) - \hat{\mathcal{R}}(\boldsymbol{\theta}))^2]. \end{aligned}$$

Setting $\delta = \frac{1}{\epsilon} \mathbb{E}_{\boldsymbol{\theta} \sim \pi} \mathbb{E}_{S \sim D^m} [(\mathcal{R}(\boldsymbol{\theta}) - \hat{\mathcal{R}}(\boldsymbol{\theta}))^2]$, now we can rewrite this inequality as follows

$$\mathbb{P}_{S \sim D^m} \left[\mathbb{E}_{\boldsymbol{\theta} \sim \pi} [(\mathcal{R}(\boldsymbol{\theta}) - \hat{\mathcal{R}}(\boldsymbol{\theta}))^2] \leq \frac{1}{\delta} \mathbb{E}_{\boldsymbol{\theta} \sim \pi} \mathbb{E}_{S \sim D^m} [(\mathcal{R}(\boldsymbol{\theta}) - \hat{\mathcal{R}}(\boldsymbol{\theta}))^2] \right] \geq 1 - \delta. \quad (18)$$

Finally, by combining 18 with 17, we complete the proof. \square

Theorem 3.2. *Under Assumption 3.1, for any confidence level $\delta \in (0, 1)$, any prior $\pi \in \mathcal{M}(\Theta)$, for any posterior $\rho \in \mathcal{M}(\Theta)$, for any $\lambda > 0$, with probability at least $1 - \delta$ we have:*

$$\text{gen}^S(\rho, S) \leq \inf_{\lambda} \left\{ \frac{\text{KL}(\rho \parallel \pi) + \ln \frac{M}{\delta}}{\lambda(M-1)} + \frac{\sum_{i=1}^{N_L} m_i \mathbb{E}_{\rho} [\Lambda_{\boldsymbol{\theta}}^{(i)}(\lambda)]}{M\lambda} \right\}. \quad (6)$$

Proof. Apply Lemma A.1 with $\varphi(\boldsymbol{\theta}, S) = M_1 \Lambda_{\boldsymbol{\theta}}^*(\text{gen}^S(\boldsymbol{\theta}, S))$, $0 < M_1 < M$, it holds with probability at least $1 - \delta$ that

$$\mathbb{E}_{\boldsymbol{\theta} \sim \rho} M_1 \Lambda_{\boldsymbol{\theta}}^{S^*}(\text{gen}^S(\boldsymbol{\theta}, S)) \leq \text{KL}(\rho \parallel \pi) + \ln \left(\frac{1}{\delta} \mathbb{E}_{S \sim \mathcal{X}^n} \mathbb{E}_{\boldsymbol{\theta} \sim \pi} e^{M_1 \Lambda_{\boldsymbol{\theta}}^{S^*}(\text{gen}^S(\boldsymbol{\theta}, S))} \right).$$

Since the prior π is independent from the training samples S , we can swap expectation using Fubini's theorem and then control $\mathbb{E}_S e^{M_1 \Lambda_{\boldsymbol{\theta}}^*(\text{gen}^S(\boldsymbol{\theta}, S))}$ for any fixed $\boldsymbol{\theta} \in \Theta$. This is done by leveraging Proposition A.3 and the surviving function theorem as presented in [6]. First, from Proposition A.3 and following the same proof as Lemma 6 in [6], we have that

$$\mathbb{P}_S (M \Lambda_{\boldsymbol{\theta}}^*(\text{gen}^S(\boldsymbol{\theta}, S)) \geq c) \leq \mathbb{P}_{X \sim \exp(1)} (X \geq c). \quad (19)$$

Since $X \sim \exp(1)$, we get $kX \sim \exp(1/k)$. Thus, multiplying the random variable $\Lambda_{\theta}^{S^*}(\text{gen}^S(\theta, S))$ by $\frac{M_1}{M}$ we have that

$$\mathbb{P}_S \left[M_1 \Lambda_{\theta}^{S^*}(\text{gen}^S(\theta, S)) \geq a \right] \leq \mathbb{P}_{X \sim \exp(\frac{M}{M_1})} (X \geq a). \quad (20)$$

Since $X \sim \exp(\frac{M}{M_1})$, we have $e^X \sim \text{Pareto}(\frac{M}{M_1}, 1)$. Thus, for any $t > 1$ we have

$$\mathbb{P}_S \left[e^{M_1 \Lambda_{\theta}^{S^*}(\text{gen}^S(\theta, S))} \geq t \right] \leq \mathbb{P}_{X \sim \text{Pareto}(\frac{M}{M_1}, 1)} (X \geq t). \quad (21)$$

Now, the term $\mathbb{E}_S e^{M_1 \Lambda_{\theta}^{S^*}(\text{gen}^S(\theta, S))}$ can be bounded by using the survival function:

$$\begin{aligned} \mathbb{E}_S e^{M_1 \Lambda_{\theta}^{S^*}(\text{gen}^S(\theta, S))} &= \int_1^{\infty} \mathbb{P}_S \left[e^{M_1 \Lambda_{\theta}^{S^*}(\text{gen}^S(\theta, S))} \geq t \right] dt \\ &\leq \int_1^{\infty} \mathbb{P}_{X \sim \text{Pareto}(\frac{M}{M_1}, 1)} (X \geq t) dt \\ &= \mathbb{E}_{X \sim \text{Pareto}(\frac{M}{M_1}, 1)} X \\ &= \frac{\frac{M}{M_1}}{\frac{M}{M_1} - 1} = \frac{M}{M - M_1}. \end{aligned}$$

Besides, note that

$$\begin{aligned} \mathbb{E}_{\theta \sim \rho} M_1 \Lambda_{\theta}^{S^*}(\text{gen}^S(\theta, S)) &= \mathbb{E}_{\theta \sim \rho} M_1 \sup_{\lambda} \{ \lambda \text{gen}^S(\theta, S) - \Lambda_{\theta}(\lambda) \} \\ &\geq M_1 \sup_{\lambda} \mathbb{E}_{\theta \sim \rho} \{ \lambda \text{gen}^S(\theta, S) - \Lambda_{\theta}(\lambda) \} \\ &= M_1 \sup_{\lambda} \left\{ \lambda \text{gen}^S(\rho, S) - \mathbb{E}_{\theta \sim \rho} [\Lambda_{\theta}(\lambda)] \right\} := M_1 \Lambda_{\rho}^*(\text{gen}^S(\rho, S)). \end{aligned}$$

So we have that

$$\mathbb{P}_S \left[M_1 \Lambda_{\rho}^*(\text{gen}^S(\rho, S)) \leq \text{KL}(\rho \parallel \pi) + \ln \frac{1}{\delta} + \ln \frac{M}{M - M_1} \right] \geq 1 - \delta.$$

Choosing $M_1 = M - 1$ then taking the generalised inverse of both sides, we get

$$\mathbb{P}_S \left[\text{gen}^S(\rho, S) \leq \inf_{\lambda} \left\{ \frac{\text{KL}(\rho \parallel \pi) + \ln \frac{1}{\delta}}{\lambda(M-1)} + \frac{\mathbb{E}_{\theta \sim \rho} [\Lambda_{\theta}(\lambda)]}{\lambda} \right\} \right] \geq 1 - \delta.$$

□

A.3 Proofs of bounds with Sobolev-smoothness assumption

Lemma A.4. *Under Assumption 3.3, for any confidence level $\delta \in (0, 1)$, any prior $\pi \in \mathcal{M}(\Theta)$, for any posterior $\rho \in \mathcal{M}(\Theta)$, with probability at least $1 - \delta$ we have:*

$$\text{gen}^S(\rho, S) \leq \sqrt{2 (\|\nabla_{\text{PIMLS}}\|_2^2) \frac{\text{KL}(\rho \parallel \pi) + \ln \frac{1}{\delta}}{M(M-1)}}, \quad (22)$$

where $\|\nabla_{\text{PIMLS}}\|_2^2 := \sum_{i=1}^{N_L} m_i C_{S,i} \mathbb{E}_{\theta \sim \rho} \mathbb{E}_{\mathbf{x} \sim D_i} \left[\|\nabla_{\mathbf{x}} \ell_i(\theta, \mathbf{x})\|_2^2 \right]$.

Proof. Applying Theorem 3.2 combining with Assumption 3.3, we have that

$$\mathbb{P}_S \left[\text{gen}^S(\rho, S) \leq \inf_{\lambda} g(\lambda) \right] \geq 1 - \delta, \quad (23)$$

where $g(\lambda) = \frac{\text{KL}(\rho|\pi) + \ln \frac{M}{\delta}}{\lambda(M-1)} + \frac{\lambda}{2} \sum_{i=1}^{N_L} \frac{m_i}{M} C_{S,i} \mathbb{E}_{\boldsymbol{\theta} \sim \rho} \mathbb{E}_{\mathbf{x}_i \sim D_i} [\|\nabla_{\mathbf{x}} \ell_i(\boldsymbol{\theta}, \mathbf{x}_i)\|_2^2]$. Since this inequality holds for all $\lambda > 0$, it also satisfies for λ that minimises the right-hand side (RHS) of Equation 23. Now solving for λ to minimise $g(\lambda)$ then plugging it to the RHS, we obtain that

$$\text{gen}^S(\rho, S) \leq \sqrt{2 (\|\nabla_{\text{PIML}_S}\|_2^2) \frac{\text{KL}(\rho|\pi) + \ln \frac{2M}{\delta}}{M(M-1)}}, \quad (24)$$

which can be finally rewritten as follows

$$\text{gen}^S(\rho, S) \leq \frac{1}{M} \sqrt{2 (\|\nabla_{\text{PIML}_S}\|_2^2) \frac{M(\text{KL}(\rho|\pi) + \ln \frac{2M}{\delta})}{M-1}}. \quad (25)$$

□

Theorem 3.5 (PAC-Bayes-Sobolev bound). *Under Assumptions 3.1, 3.3 and 3.4, for any confidence level $\delta \in (0, 1)$, any prior $\pi \in \mathcal{M}(\Theta)$, for any posterior $\rho \in \mathcal{M}(\Theta)$, with probability at least $1 - \delta$ we have:*

$$\text{gen}^S(\rho, S) \leq \frac{1}{M} \sqrt{2 \|\hat{\nabla}_{\text{PIML}_S}(\rho)\|_2^2 K(\rho, \pi, \delta) + L_{\text{PIML}_S} K(\rho, \pi, \delta)^{\frac{3}{2}}}, \quad (7)$$

where $\|\hat{\nabla}_{\text{PIML}_S}(\rho)\|_2^2 := \sum_{i=1}^{N_L} C_{S,i} \mathbb{E}_{\boldsymbol{\theta} \sim \rho} \sum_{j=1}^{m_i} [\|\nabla_{\mathbf{x}} \ell_i(\boldsymbol{\theta}, \mathbf{x}_{i,j})\|_2^2]$; $K(\rho, \pi, \delta) := \frac{M(\text{KL}(\rho|\pi) + \ln \frac{2M}{\delta})}{M-1}$ and $L_{\text{PIML}_S} := \sqrt{2 \sum_{i=1}^{N_L} m_i C_{S,i}^2 L_i^2}$.

Proof. First, applying Lemma A.4, with probability at least $1 - \frac{\delta}{2}$, it holds that

$$\text{gen}^S(\rho, S) \leq \frac{1}{M} \sqrt{2 (\|\nabla_{\text{PIML}_S}\|_2^2) \frac{M(\text{KL}(\rho|\pi) + \ln \frac{2M}{\delta})}{M-1}}. \quad (26)$$

Now we need to replace the true gradient term $\|\nabla_{\text{PIML}_S}\|_2^2$ by its corresponding empirical version. By Assumption 3.4, $\|\nabla_{\mathbf{x}} \ell_i(\boldsymbol{\theta}, \mathbf{x})\|_2^2 \leq L_i$ therefore $\|\nabla_{\mathbf{x}} \ell_i(\boldsymbol{\theta}, \mathbf{x})\|_2^2$ is $\frac{L_i^2}{4}$ -sub-gaussian, i.e., ,

$$\mathbb{E}_{\mathbf{x}_i \sim D_i} e^{\lambda C_{S,i} (\mathbb{E}_{\mathbf{x}_i \sim D_i} \|\nabla_{\mathbf{x}} \ell_i(\boldsymbol{\theta}, \mathbf{x})\|_2^2 - \|\nabla_{\mathbf{x}} \ell_i(\boldsymbol{\theta}, \mathbf{x})\|_2^2)} \leq e^{\frac{\lambda^2 C_{S,i}^2 L_i^2}{8}}. \quad (27)$$

Applying Theorem 3.2 with the "losses" $C_i \|\nabla_{\mathbf{x}} \ell_i(\boldsymbol{\theta}, \mathbf{x})\|_2^2$ then combining with Equation 27 to bound the CGF, we obtain with probability at least $1 - \frac{\delta}{2}$ that

$$\|\nabla_{\text{PIML}_S}(\rho)\|_2^2 \leq \|\hat{\nabla}_{\text{PIML}_S}(\rho)\|_2^2 + \inf_{\lambda} \left\{ \frac{M(\text{KL}(\rho|\pi) + \ln \frac{2M}{\delta})}{\lambda(M-1)} + \frac{\lambda \sum_{i=1}^{N_L} m_i C_{S,i}^2 L_i^2}{8} \right\}. \quad (28)$$

Solving λ to minimise the RHS, we have that:

$$\|\nabla_{\text{PIML}_S}(\rho)\|_2^2 \leq \|\hat{\nabla}_{\text{PIML}_S}(\rho)\|_2^2 + \sqrt{\frac{M(\text{KL}(\rho|\pi) + \ln \frac{2M}{\delta})}{2(M-1)} \sum_{i=1}^{N_L} m_i C_{S,i}^2 L_i^2}. \quad (29)$$

Finally combining 29 and 26 via a union bound, we complete the proof. □

A.4 Proofs of bounds with Poincaré-smoothness assumption

Lemma A.5. *Under Assumption 3.6, for any confidence level $\delta \in (0, 1)$, any prior $\pi \in \mathcal{M}(\Theta)$, for any posterior $\rho \in \mathcal{M}(\Theta)$, for any $\lambda > 0$, for $\alpha > 1$ with probability at least $1 - \delta$ we have:*

$$\text{gen}(\rho, S) \leq \sqrt{\frac{\bar{D} \|\nabla_{\text{PIML}_P}\|_2^2}{\delta}}, \quad (30)$$

$$\text{gen}^S(\rho, S) \leq \frac{1}{M} \sqrt{\frac{\bar{D} \|\nabla_{\text{PIMLP}}^S(\pi)\|_2^2}{\delta}}, \quad (31)$$

where $\|\nabla_{\text{PIMLP}}(\pi)\|_2^2 := \sum_{i=1}^{N_L} \frac{C_{P,i}}{m_i} \mathbb{E}_{\boldsymbol{\theta} \sim \pi} \mathbb{E}_{\mathbf{x} \sim D_i} \|\nabla \ell_i(\boldsymbol{\theta}, \mathbf{x})\|_2^2$ and $\|\nabla_{\text{PIMLP}}(\pi)\|_2^2 := \sum_{i=1}^{N_L} m_i C_{P,i} \mathbb{E}_{\boldsymbol{\theta} \sim \pi} \mathbb{E}_{\mathbf{x} \sim D_i} \|\nabla \ell_i(\boldsymbol{\theta}, \mathbf{x})\|_2^2$.

Proof. We proceed by directly applying Theorem 2.1 with the corresponding composite loss functions. First, let us consider $\varphi = \text{gen}(\boldsymbol{\theta}, S)$. Leveraging the i.i.d assumption between training points and Poincaré assumption we have

$$\begin{aligned} \mathbb{E}_{\boldsymbol{\theta} \sim \pi} \mathbb{E}_{\mathbf{x}_{i,j} \sim D_i} (\text{gen}(\boldsymbol{\theta}, S))^2 &= \mathbb{E}_{\boldsymbol{\theta} \sim \pi} \mathbb{E}_{\mathbf{x}_{i,j} \sim D_i} \left(\sum_{i=1}^{N_L} \frac{1}{m_i} \sum_{j=1}^{m_i} (\mathcal{R}_i(\boldsymbol{\theta}) - \ell_i(\boldsymbol{\theta}, \mathbf{x}_{i,j})) \right)^2 \\ &= \mathbb{E}_{\boldsymbol{\theta} \sim \pi} \sum_{i=1}^{N_L} \sum_{j=1}^{m_i} \mathbb{E}_{\mathbf{x}_{i,j} \sim D_i} \left(\frac{\mathcal{R}_i(\boldsymbol{\theta}) - \ell_i(\boldsymbol{\theta}, \mathbf{x}_{i,j})}{m_i} \right)^2 \\ &= \mathbb{E}_{\boldsymbol{\theta} \sim \pi} \sum_{i=1}^{N_L} \frac{1}{m_i} \mathbb{V}[\ell_i(\boldsymbol{\theta})] \\ &\leq \mathbb{E}_{\boldsymbol{\theta} \sim \pi} \sum_{i=1}^{N_L} \frac{C_{P,i}}{m_i} \mathbb{E}_{\mathbf{x} \sim D_i} \|\nabla_{\mathbf{x}} \ell_i(\boldsymbol{\theta}, \mathbf{x})\|_2^2 \quad (\text{Assumption 3.6}), \end{aligned}$$

where the second equality comes from Assumption 3.1.

Similarly, for Inequality 31, let us consider the sample-centric generalisation gap $\varphi = M\text{gen}^S(\boldsymbol{\theta}, S)$. Leveraging the i.i.d assumption between training points and Poincaré assumption we also have

$$\begin{aligned} \mathbb{E}_{\boldsymbol{\theta} \sim \pi} \mathbb{E}_{\mathbf{x}_{i,j} \sim D_i} (M\text{gen}^S(\boldsymbol{\theta}, S))^2 &= \mathbb{E}_{\boldsymbol{\theta} \sim \pi} \mathbb{E}_{\mathbf{x}_{i,j} \sim D_i} \left(\sum_{i=1}^{N_L} \sum_{j=1}^{m_i} (\mathcal{R}_i(\boldsymbol{\theta}) - \ell_i(\boldsymbol{\theta}, \mathbf{x}_{i,j})) \right)^2 \\ &= \mathbb{E}_{\boldsymbol{\theta} \sim \pi} \sum_{i=1}^{N_L} \sum_{j=1}^{m_i} \mathbb{E}_{\mathbf{x}_{i,j} \sim D_i} (\mathcal{R}_i(\boldsymbol{\theta}) - \ell_i(\boldsymbol{\theta}, \mathbf{x}_{i,j}))^2 \\ &= \mathbb{E}_{\boldsymbol{\theta} \sim \pi} \sum_{i=1}^{N_L} m_i \mathbb{V}[\ell_i(\boldsymbol{\theta})] \\ &\leq \mathbb{E}_{\boldsymbol{\theta} \sim \pi} \sum_{i=1}^{N_L} m_i C_{P,i} \mathbb{E}_{\mathbf{x} \sim D_i} \|\nabla_{\mathbf{x}} \ell_i(\boldsymbol{\theta}, \mathbf{x})\|_2^2 \quad (\text{Assumption 3.6}). \end{aligned}$$

Then by simply plugging these results into Theorem 2.1, we finish the proof. \square

Theorem 3.7 (PAC-Bayes-Poincaré bounds). *Under Assumptions 3.1, 3.6 and 3.4, for any confidence level $\delta \in (0, 1)$, any prior $\pi \in \mathcal{M}(\Theta)$, for any posterior $\rho \in \mathcal{M}(\Theta)$, for any $\lambda > 0$, with probability at least $1 - \delta$ we have:*

$$\text{gen}(\rho, S) \leq \sqrt{\frac{(2\|\hat{\nabla}_{\text{PIMLP}}(\pi)\|_2^2 + L_{\text{PIMLP}} K(\delta)^{\frac{1}{2}}) \bar{D}}{\delta}}, \quad (8)$$

$$\text{gen}^S(\rho, S) \leq \frac{1}{M} \sqrt{\frac{(2\|\hat{\nabla}_{\text{PIMLP}}^S(\pi)\|_2^2 + L_{\text{PIMLP}}^S K(\delta)^{\frac{1}{2}}) \bar{D}}{\delta}}, \quad (9)$$

where $\|\hat{\nabla}_{\text{PIML}_P}(\pi)\|_2^2 := \sum_{i=1}^{N_L} \frac{C_{P,i}}{m_i^2} \mathbb{E}_{\boldsymbol{\theta} \sim \pi} \sum_{j=1}^{m_i} \|\nabla \ell_i(\boldsymbol{\theta}, \mathbf{x}_{i,j})\|_2^2$; $\|\hat{\nabla}_{\text{PIML}_P^S}(\pi)\|_2^2 := \sum_{i=1}^{N_L} C_{P,i} \mathbb{E}_{\boldsymbol{\theta} \sim \pi} \sum_{j=1}^{m_i} \|\nabla \ell_i(\boldsymbol{\theta}, \mathbf{x}_{i,j})\|_2^2$; $L_{\text{PIML}_P} := \sqrt{2 \sum_{i=1}^{N_L} \frac{C_{P,i}^2 L_i^2}{m_i^3}}$; $L_{\text{PIML}_P^S} := \sqrt{2 \sum_{i=1}^{N_L} m_i C_{P,i}^2 L_i^2}$; and $K(\delta) := \frac{M \ln \frac{2M}{\delta}}{M-1}$.

Proof. The proof for these two inequalities can be done following the same argument as the proof of Theorem 3.5. First, applying Lemma A.5 with $\delta' = \frac{\delta}{2}$ we have that

$$\text{gen}(\rho, S) \leq \sqrt{\frac{2}{\delta} \bar{D} \|\nabla_{\text{PIML}_P}(\boldsymbol{\theta})\|_2^2}, \quad (32)$$

$$\text{gen}^S(\rho, S) \leq \frac{1}{M} \sqrt{\frac{2}{\delta} \bar{D} \|\nabla_{\text{PIML}_P^S}(\boldsymbol{\theta})\|_2^2}. \quad (33)$$

Exploiting the Lipschitzness assumption like in the proof of Theorem 3.5, we obtain that

$$\mathbb{E}_{\mathbf{x}_i \sim D_i} e^{\lambda \frac{C_{P,i}}{m_i} (\mathbb{E}_{\mathbf{x}_i \sim D_i} \|\nabla_{\mathbf{x}} \ell_i(\boldsymbol{\theta}, \mathbf{x})\|_2^2 - \|\nabla_{\mathbf{x}} \ell_i(\boldsymbol{\theta}, \mathbf{x})\|_2^2)} \leq e^{\frac{\lambda^2 C_{P,i}^2 L_i^2}{8m_i^4}}, \quad (34)$$

$$\mathbb{E}_{\mathbf{x}_i \sim D_i} e^{\lambda C_{P,i} (\mathbb{E}_{\mathbf{x}_i \sim D_i} \|\nabla_{\mathbf{x}} \ell_i(\boldsymbol{\theta}, \mathbf{x})\|_2^2 - \|\nabla_{\mathbf{x}} \ell_i(\boldsymbol{\theta}, \mathbf{x})\|_2^2)} \leq e^{\frac{\lambda^2 C_{P,i}^2 L_i^2}{8}}. \quad (35)$$

Now respectively plugging 34, and 35 into Theorem 3.2 with the losses $\frac{C_{P,i}}{m_i^2} \|\nabla_{\mathbf{x}} \ell_i(\boldsymbol{\theta}, \mathbf{x})\|_2^2$, and $C_{P,i} \|\nabla_{\mathbf{x}} \ell_i(\boldsymbol{\theta}, \mathbf{x})\|_2^2$, then solving for λ , we obtain with probability at least $1 - \frac{\delta}{2}$ that

$$\|\nabla_{\text{PIML}_P}(\rho')\|_2^2 \leq \|\hat{\nabla}_{\text{PIML}_P}(\rho')\|_2^2 + \sqrt{\frac{M(\text{KL}(\rho' \|\pi) + \ln \frac{2M}{\delta})}{2(M-1)} \sum_{i=1}^{N_L} \frac{C_{P,i}^2 L_i^2}{m_i^3}}, \quad (36)$$

$$\|\nabla_{\text{PIML}_P^S}(\rho')\|_2^2 \leq \|\hat{\nabla}_{\text{PIML}_P^S}(\rho')\|_2^2 + \sqrt{\frac{M(\text{KL}(\rho' \|\pi) + \ln \frac{2M}{\delta})}{2(M-1)} \sum_{i=1}^{N_L} m_i C_{P,i}^2 L_i^2}. \quad (37)$$

Setting $\rho' = \pi$, we obtain that

$$\|\nabla_{\text{PIML}_P}(\pi)\|_2^2 \leq \|\hat{\nabla}_{\text{PIML}_P}(\pi)\|_2^2 + \sqrt{\frac{M \ln \frac{2M}{\delta}}{2(M-1)} \sum_{i=1}^{N_L} \frac{C_{P,i}^2 L_i^2}{m_i^3}}, \quad (38)$$

$$\|\nabla_{\text{PIML}_P^S}(\pi)\|_2^2 \leq \|\hat{\nabla}_{\text{PIML}_P^S}(\pi)\|_2^2 + \sqrt{\frac{M \ln \frac{2M}{\delta}}{2(M-1)} \sum_{i=1}^{N_L} m_i C_{P,i}^2 L_i^2}. \quad (39)$$

Combining 38 with 32, 39 with 33 via a union bound, then rewriting it using the above notations, we complete the proof. \square

B Additional Information on Experiment Setup, Implementation and Results

B.1 Benchmarks

1D-Wave. This problem considers a one-dimensional hyperbolic partial differential equation (PDE) that is commonly used as a benchmark for wave propagation phenomena. The governing equation is ¹

$$\begin{aligned} \frac{\partial^2 u}{\partial t^2} - 4 \frac{\partial^2 u}{\partial x^2} &= 0, & x \in (0, 1), t \in (0, 1), \\ u(x, 0) &= \sin(\pi x) + \frac{1}{2} \sin(\beta \pi x), & x \in [0, 1], \\ \frac{\partial u(x, 0)}{\partial t} &= 0, & x \in [0, 1], \\ u(0, t) &= u(1, t) = 0, & t \in [0, 1]. \end{aligned} \quad (40)$$

The corresponding analytic solution is

$$u(x, t) = \sin(\pi x) \cos(2\pi t) + \frac{1}{2} \sin(\beta \pi x) \cos(2\beta \pi t). \quad (41)$$

In our experiments, we set $\beta = 4$. Despite its relatively simple form, this problem poses challenges for physics-informed neural networks (PINNs) due to the presence of multiple frequency components in the solution. As described above, we have five different equations, therefore in the experiment parts, for clarity, we denote the physical loss terms as follows:

$$\begin{aligned} \ell_p(\boldsymbol{\theta}, \mathbf{x}) &= \left(\frac{\partial^2 u_{\boldsymbol{\theta}}}{\partial t^2} - 4 \frac{\partial^2 u_{\boldsymbol{\theta}}}{\partial x^2} \right)^2, \\ \ell_{ic}(\boldsymbol{\theta}, \mathbf{x}) &= \left(u_{\boldsymbol{\theta}}(x, 0) - \sin(\pi x) - \frac{1}{2} \sin(\beta \pi x) \right)^2, \\ \ell_{ig}(\boldsymbol{\theta}, \mathbf{x}) &= \left(\frac{\partial u_{\boldsymbol{\theta}}(x, 0)}{\partial t} \right)^2, \\ \ell_{b_1}(\boldsymbol{\theta}, \mathbf{x}) &= (u_{\boldsymbol{\theta}}(0, t))^2, \\ \ell_{b_2}(\boldsymbol{\theta}, \mathbf{x}) &= (u_{\boldsymbol{\theta}}(1, t))^2 \end{aligned} \quad (42)$$

As depicted in Figure 3, the solution map is relatively smoother compared to the other two problems, thereby it is easier for models to achieve small data-fidelity error. However, the equation contains second-order derivatives which is the main obstacle both in terms of learning and computation. Indeed, the loss ℓ_p and its derivative $\|\nabla_{\boldsymbol{\theta}} \ell_p\|$ are the dominant terms in both empirical loss and the complexity of the bound.

1D-Reaction. This problem considers a one-dimensional nonlinear ordinary differential equation (ODE) that arises in the modeling of chemical reactions. The equation is given by

$$\begin{aligned} \frac{\partial u}{\partial t} - \kappa u(1 - u) &= 0, & x \in (0, 2\pi), t \in (0, 1), \\ u(x, 0) &= \exp\left(-\frac{(x - \pi)^2}{2(\pi/4)^2}\right), & x \in [0, 2\pi], \\ u(0, t) &= u(2\pi, t), & t \in [0, 1]. \end{aligned} \quad (43)$$

The corresponding analytical solution is

$$u(x, t) = \frac{h(x)e^{\kappa t}}{h(x)e^{\kappa t} + 1 - h(x)}, \quad (44)$$

¹For clarity, π denotes the numeric constant $\pi \approx 3.14$ in this section, to avoid confusion with the prior distribution in the bounds.

where

$$h(x) = \exp\left(-\frac{(x - \pi)^2}{2(\pi/4)^2}\right). \quad (45)$$

In our experiments, we set $\kappa = 5$. We consider the following three physical losses:

$$\begin{aligned} \ell_p(\boldsymbol{\theta}, \mathbf{x}) &= \left(\frac{\partial u_{\boldsymbol{\theta}}}{\partial t} - \kappa u_{\boldsymbol{\theta}}(1 - u_{\boldsymbol{\theta}})\right)^2, \\ \ell_{ic}(\boldsymbol{\theta}, \mathbf{x}) &= (u_{\boldsymbol{\theta}}(x, 0) - h(x))^2, \\ \ell_b(\boldsymbol{\theta}, \mathbf{x}) &= (u_{\boldsymbol{\theta}}(0, t) - u_{\boldsymbol{\theta}}(2\pi, t))^2. \end{aligned} \quad (46)$$

This problem draws much attention as early PINN training suffers failure mode due to the presence of the non-linear term of the equation. As shown in Figure 3, the solution map contains sharp boundaries in the center high-value area, making it hard for being learned by neural networks. Therefore, the data-fidelity loss ℓ_d slightly dominates over the PDE residual loss ℓ_p in this case, as shown by the empirical risks in Table 3. However, as the total empirical risk is very small ($\sim 10^{-3}$), the complexity term is the most dominant in the bound, it will likely favor posterior extremely close to the prior and the self-bounding-aware algorithm become useless. To deal with this, we amplify each loss term by a factor of 100 and use this scaled version during the entire computation of Algorithm 1. Once the final bound on the scaled risks is computed, we just divide it by 100 to obtain the bound on the original risks.

Convection. This problem considers a hyperbolic partial differential equation (PDE) that serves as a standard benchmark for transport-dominated dynamics [39], also known as advection. The governing equation is

$$\begin{aligned} \frac{\partial u}{\partial t} + \beta \frac{\partial u}{\partial x} &= 0, & x \in (0, 2\pi), t \in (0, 1), \\ u(x, 0) &= \sin(x), & x \in [0, 2\pi], \\ u(0, t) &= u(2\pi, t), & t \in [0, 1]. \end{aligned} \quad (47)$$

The corresponding analytic solution is

$$u(x, t) = \sin(x - \beta t). \quad (48)$$

In our experiments, we set $\beta = 50$. Despite the simple closed-form expression, this problem remains challenging for physics-informed neural networks (PINNs) due to the high-frequency and rapidly propagating solution features. As this problem has similar equation forms like 1D-Reaction, we consider the following physical losses in the experiments:

$$\begin{aligned} \ell_p(\boldsymbol{\theta}, \mathbf{x}) &= \left(\frac{\partial u_{\boldsymbol{\theta}}}{\partial t} + \beta \frac{\partial u_{\boldsymbol{\theta}}}{\partial x}\right)^2, \\ \ell_{ic}(\boldsymbol{\theta}, \mathbf{x}) &= (u_{\boldsymbol{\theta}}(x, 0) - \sin(x))^2, \\ \ell_b(\boldsymbol{\theta}, \mathbf{x}) &= (u_{\boldsymbol{\theta}}(0, t) - u_{\boldsymbol{\theta}}(2\pi, t))^2. \end{aligned} \quad (49)$$

Since the total empirical risk is relatively small ($\sim 10^{-2}$), we also scale the losses with a factor of 10 during the entire computation of Algorithm 1, then divide the resulting scaled bound by 10 to obtain the bound on the original risk.

B.2 Empirical observations on gradient distribution

We empirically examine the feasibility of the bounds introduced above, which require the existence of finite constants ensuring that the proposed inequalities hold uniformly over the hypothesis class. In particular, these assumptions implicitly rely on bounding the Lipschitz continuity of the model, i.e., controlling the supremum of the gradient norm over the parameter space.

To probe this requirement, we focus on the empirical behavior of the Lipschitz constant, approximated by the maximum gradient norm. Starting from a trained model $\boldsymbol{\theta}_\pi$, for each distance, we generate

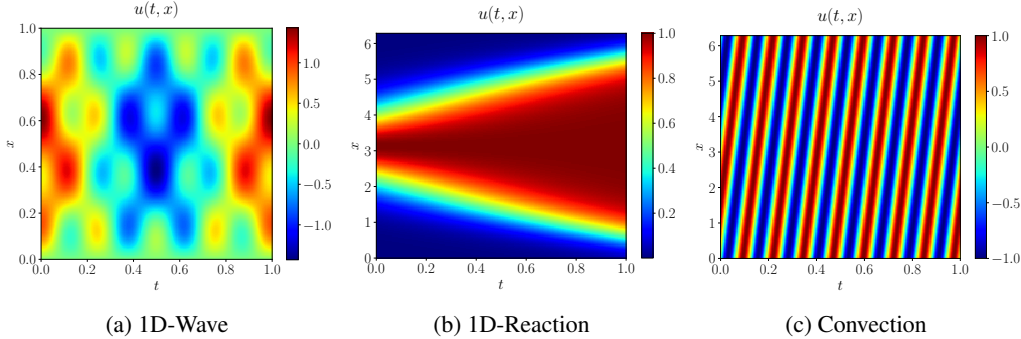


Figure 3: Visualisation of the solution u for the three benchmarks.

100 perturbed models by arbitrarily sampling the direction, and evaluate the corresponding gradient norms. This procedure provides a direct estimate of how the effective Lipschitz constant evolves as one moves away from a well-trained solution. The results are reported in Figure 4, where we plot the maximum observed gradient norm of the data-fidelity loss ℓ_d and PDE loss ℓ_p as a function of the distance $\|\theta_\pi - \theta\|_2$. Our observations reveal a pronounced growth of the gradient norm with respect to the distance from the trained model. In particular, the estimated Lipschitz constant increases rapidly and exhibits unbounded behavior as one explores regions further away in parameter space. Even for moderate perturbations at distance of 1, the gradient norm of the PDE loss can already reach a magnitude of 10^8 . This leads to significantly loosened bounds, which may become vacuous in practice. As a consequence, any constant chosen to uniformly bound the gradient over such regions must be extremely large, effectively diverging when the domain is not restricted to a small neighborhood of the trained model.

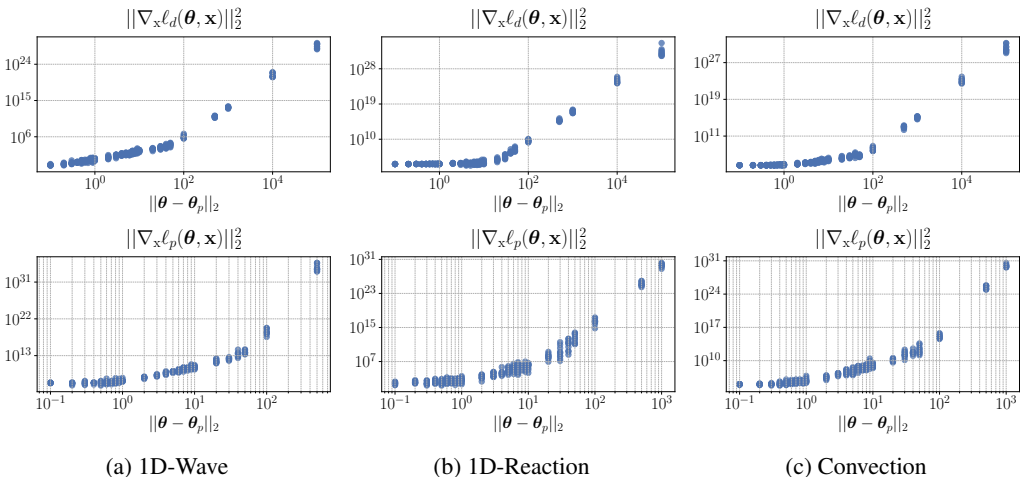


Figure 4: Gradient norm of the losses ℓ_d and ℓ_p w.r.t the inputs in three benchmarks.

These observations suggest that, to obtain tighter bounds, it is crucial to restrict attention to local neighborhoods of a well-trained model (used as the prior). In particular, low bound values arise when the posterior does not diverge significantly from the prior. Therefore, estimating the relevant constants within a ball centered at the prior—with radius large enough to contain the posterior—suffices to ensure the conditions are satisfied in practice.

B.3 Leveraging local loss boundedness for constant estimation

Although the input-gradient of losses explodes quickly, we empirically observe that the losses themselves remain small and exhibit limited variability in the neighborhood of the learned prior model. Figure 5 shows that in all three benchmarks, the dominant losses ℓ_d and ℓ_p are much smaller

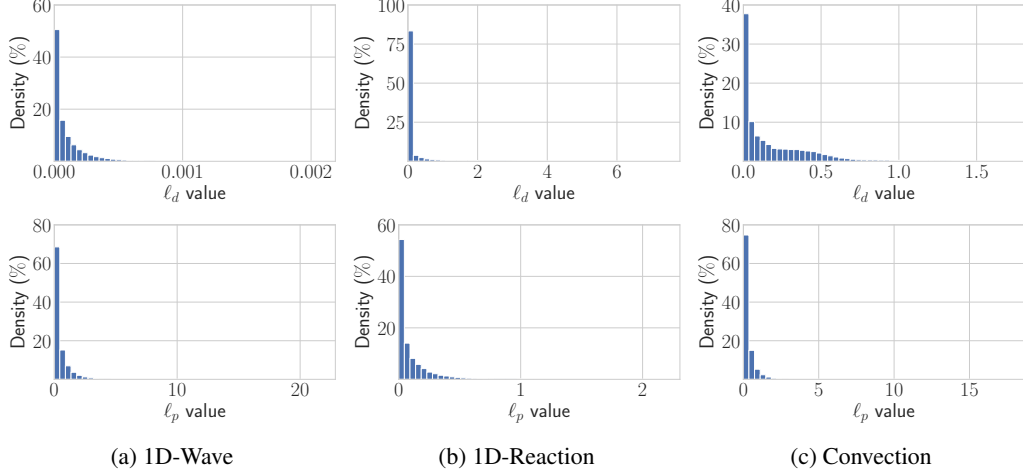


Figure 5: Distribution of ℓ_d and ℓ_p around well-trained models in three benchmarks.

than 100. Therefore, if we apply a clipping at that value, it almost surely has no impact to the loss value. Nevertheless, such clipping is highly beneficial when estimating those constants, as it ensures that the losses remain locally bounded in the neighborhood of the prior model, which in turn bounds their variances and stabilizes the associated CGF. As a consequence, we can also clip input-gradients while always being able to find constants satisfying the Sobolev and Poincaré assumptions. It is now necessary to identify proper constants that tighten the bounds.

There is an inherent trade-off between the clipping thresholds L_i and the resulting Sobolev constant $C_{S,i}$ and Poincaré constant $C_{P,i}$. Concretely, reducing L_i will result in larger $C_{S,i}$ and $C_{P,i}$, while choosing excessively large L_i will produce loose bounds. Therefore, it is desirable to select L_i that reduces the bound values in Theorem 3.5 and 3.7, i.e., by minimising those constants along with the quantities $L_i C_{S,i}$ and $L_i C_{P,i}$. For this purpose, we make use of a collection of calibration set S_{calib} disjoint to S_{prior} and S_{post} , to compute the CGF, the variance of the losses and the expected gradient.

Figure 6 shows the curve $\frac{2\Lambda_{\theta}^{(i)}(\lambda)}{\lambda^2 \mathbb{E}_{\mathbf{x} \sim D} [\|\nabla_{\mathbf{x}} \ell_i(\theta, \mathbf{x})\|_2^2]}$ at different distances and we can see that the ratio of interest generally increases with distance, but decreases with λ . Besides, by using L'Hopital's rule, we have that $\lim_{\lambda \rightarrow 0^+} \frac{2\Lambda_{\theta}^{(i)}(\lambda)}{\lambda^2 \mathbb{E}_{\mathbf{x} \sim D} [\|\nabla_{\mathbf{x}} \ell_i(\theta, \mathbf{x})\|_2^2]} = \frac{\mathbb{V}_{\mathbf{x} \sim D} [\ell_i(\theta, \mathbf{x})]}{\mathbb{E}_{\mathbf{x} \sim D} \|\nabla \ell_i(\theta, \mathbf{x})\|_2^2}$, which directly relates to the quantity of interest of the Poincaré assumption. Therefore, we can simply restrict the search to L_i and $C_{P,i}$ only. Figure 7 then shows that $\frac{\mathbb{V}_{\mathbf{x} \sim D} [\ell_i(\theta, \mathbf{x})]}{\mathbb{E}_{\mathbf{x} \sim D} \|\nabla \ell_i(\theta, \mathbf{x})\|_2^2}$ generally increase with distance, therefore we can restrict the search of L_i by looking at the value of the ratios at distance 1.

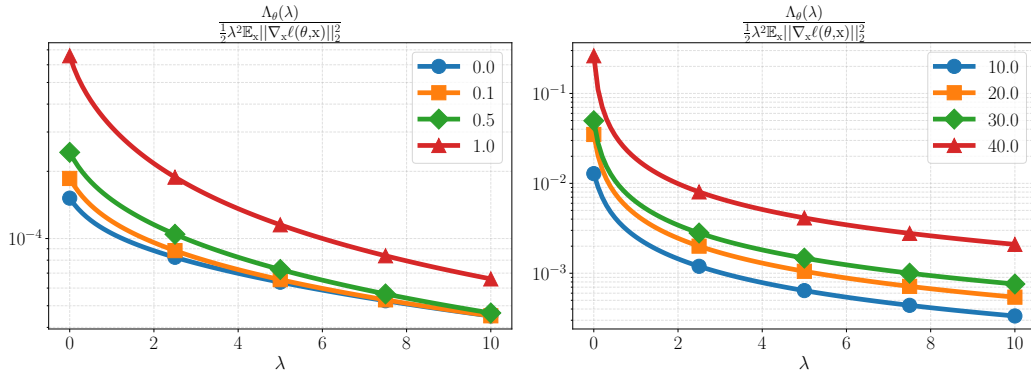


Figure 6: Curves of $\frac{\Lambda_{\theta}^{(i)}(\lambda)}{0.5\lambda^2 \mathbb{E}_{\mathbf{x} \sim D} [\|\nabla_{\mathbf{x}} \ell_i(\theta, \mathbf{x})\|_2^2]}$ at different distances $\|\theta_{\pi} - \theta\|_2$ between θ and the prior model θ_{π} . Note that θ is sampled at random directions.

The search is described in lines 6-11 of Algorithm 1. In details, for each loss i , the function $C_p(\tau, 1, N_{draw})$ will samples N_{draw} models at distance 1, compute the ratio $\frac{\mathbb{V}_{\mathbf{x} \sim D}[\ell_i(\boldsymbol{\theta}, \mathbf{x})]}{\mathbb{E}_{\mathbf{x} \sim D} \|\nabla \ell_i(\boldsymbol{\theta}, \mathbf{x})\|_2^2}$ when the gradient is clipped at τ , then return the maximum value as \mathcal{S}_τ . This form a set \mathcal{S}_τ . Here we set τ from 1 to 10^4 . Next, the function $\text{Smallest}_k(\mathcal{S}_\tau)$ select the threshold candidates corresponding to k -smallest values in \mathcal{S}_τ , and return a list of indices \mathcal{L} . Then we choose the one with smallest $C_p(\tau, 1, N_{draw})$ as L_i . This scheme allows us to avoid over-loose bounds, by limiting the factors that control the bounds ($L_i C_{S,i}$, $L_i C_{P,i}$ and $C_{P,i}$, $C_{S,i}$). Finally, from the chosen L_i , we randomly sample N_{draw} models one more time to refine the search, and determine the value of $(C_{P,i}, C_{S,i})$ by choosing the maximum value at radius under or equal to 1. This method enables an effective estimation of the constants without costly optimization procedure. However, as the search heavily relies on the draw of models at random directions, the resulting constants may changes from one run to another, although they generally have the same order of magnitude. We thus set random seeds to obtain deterministic results. Table 2 presents an example of the set of constants estimated in three benchmark. Although having the same nature of approximation error, the data-fidelity loss ℓ_d and the initial condition loss ℓ_{ic} have very different constant values. It is due to the fact that the interior region is more difficult to learn, and the loss exhibits much higher gradient there than at the initial/boundary area. As a consequence, the Sobolev and Poincaré constants are much larger in the latter case. Therefore, using ℓ_{ic} to alleviate the lack of observation calibration data will likely inflate the bounds.

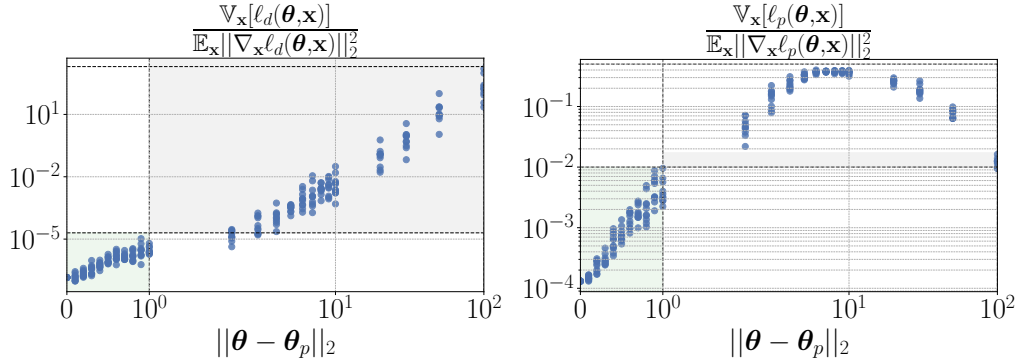


Figure 7: Scatter plots of $\frac{\mathbb{V}_{\mathbf{x}}[\ell(\boldsymbol{\theta}, \mathbf{x})]}{\mathbb{E}_{\mathbf{x} \sim D} \|\nabla_{\mathbf{x}} \ell(\mathbf{x})\|_2^2}$ for ℓ_d and ℓ_p . Here the Assumption hold with $C_{P_d} = 2e-5$ and $C_{P_d} = 1e-2$ within the radius of 1, i.e., $\|\boldsymbol{\theta} - \boldsymbol{\theta}_\pi\|_2 \leq 1$. In the case of ℓ_p , we see that the ratio decrease when $\|\boldsymbol{\theta} - \boldsymbol{\theta}_\pi\|_2 \geq 10$, since the loss values are clipped and its variance is therefore decreased, while the gradient do not decrease with distance.

B.4 Details on the self-bounding-aware algorithms and the computation of the bounds

Note that in a balanced setting (i.e., $m_i = m$, $\forall i$), the sample-centric bounds on $\text{gen}^S(\rho, S)$ can be rewritten as an equally-weighted bound, by simply dividing both sides to m . This way, we can learn to directly minimise the bound (**self-bounding**) through the following objectives corresponding to the bound in theorems 3.5 and 3.7:

$$\sum_{i=1}^{N_L} \hat{\mathcal{R}}_{ic}(\boldsymbol{\theta}') + \sqrt{2 \sum_{i=1}^{N_L} \frac{C_{S,i}}{m^2} \sum_{j=1}^m \left[\|\nabla_{\mathbf{x}} \ell_i(\boldsymbol{\theta}', \mathbf{x}_{i,j})\|_2^2 \right] K(\boldsymbol{\theta}_\rho) + \frac{L_{\text{PIMLS}}}{m^2} K(\boldsymbol{\theta}_\rho)^{\frac{3}{2}}}, \quad (50)$$

$$\sum_{i=1}^{N_L} \hat{\mathcal{R}}_{ic}(\boldsymbol{\theta}') + \sqrt{\frac{\left(2 \sum_{i=1}^{N_L} \frac{C_{P,i}}{m^2} \sum_{j=1}^m \|\nabla \ell_i(\pi, \mathbf{x}_{i,j})\|_2^2 + L_{\text{PIMLP}} K(\boldsymbol{\theta}_\pi) \right)}{\delta}} e^{\left(\frac{\|\boldsymbol{\theta}_\rho - \boldsymbol{\theta}_\pi\|_2^2}{\sigma^2} \right)}, \quad (51)$$

where $\|\nabla \ell_i(\pi, \mathbf{x}_{i,j})\|_2^2 := \mathbb{E}_{\boldsymbol{\theta} \sim \pi} \|\nabla \ell_i(\boldsymbol{\theta}, \mathbf{x}_{i,j})\|_2^2$.

In the general unbalanced setting, we only obtain a sample-weighted bound $\mathcal{U}_{\text{PIML}}^S(\rho)$ rather than the target equally-weighted bound $\mathcal{U}_{\text{PIML}}(\rho)$. Therefore, we have to solve an optimization problem to obtain the target bound from the sample-weighted one. For convenience, let us denote

Table 2: An example of the constants estimated by our selection algorithm.

Constant	1D-Wave	1D-Reaction	Convection
L_d	1	30	400
$C_{S,d}$	7e-6	2e-1	7e-4
$C_{P,d}$	2e-5	1e-1	7e-4
L_p	4.4e3	30	6.2e3
$C_{S,p}$	2e-2	5e-1	2e-2
$C_{P,p}$	2e-1	8e-1	4e-3
L_{ic}	2	5	4
$C_{S,ic}$	3e-2	2	8e-1
$C_{P,ic}$	4e-2	2	9e-1
L_{ig}	10	-	-
$C_{S,ig}$	7e-3	-	-
$C_{P,ig}$	2e-2	-	-
L_{b_1}	4	-	-
C_{S,b_1}	2e-2	-	-
C_{P,b_1}	2e-2	-	-
L_{b_2}	3	-	-
C_{S,b_2}	2e-2	-	-
C_{P,b_2}	1e-5	-	-
L_b	-	2	10
$C_{S,b}$	-	1e-1	2e-3
$C_{P,b}$	-	1e-1	2e-3

$\|\hat{\nabla}_{\mathbf{x}} \ell_i(\rho')\|_2^2 := \mathbb{E}_{\boldsymbol{\theta} \sim \rho'} \frac{1}{m_i} \sum_{j=1}^{m_i} \|\hat{\nabla}_{\mathbf{x}} \ell_i(\boldsymbol{\theta}, \mathbf{x}_{i,j})\|_2^2$ and $K_i(\rho', \pi, \delta) = \frac{\text{KL}(\rho' \|\pi) + \ln \frac{2m_i}{\delta}}{m_i - 1}$ for an arbitrary distribution ρ' over model parameters. Then we can formulate the following linear optimisation problem to obtain the bound $\mathcal{U}_{\text{PIML}}(\rho)$ from sample-weighted bound $\mathcal{U}_{\text{PIML}}^{\text{S}}(\rho)$:

$$\begin{aligned} \max \sum_{i=1}^{N_L} \mathcal{R}_i(\rho) \quad \text{s.t.} \\ \mathcal{R}_i(\rho) \leq \hat{\mathcal{R}}_i(\rho) + \mathcal{U}_i(\rho), \\ \sum_{i=1}^{N_L} \frac{m_i}{M} \mathcal{R}_i(\rho) \leq \sum_{i=1}^{N_L} \frac{m_i}{M} \hat{\mathcal{R}}_i(\rho) + \mathcal{U}^{\text{S}}(\rho), \end{aligned} \tag{52}$$

whose constraints hold simultaneously with probability at least $1 - \delta$ over the draw of the collection posterior set S_{post} . Here $\mathcal{U}_i(\rho) := \sqrt{2C_{S,i} \left[\|\hat{\nabla}_{\mathbf{x}} \ell_i(\rho)\|_2^2 \right] K(\rho, \pi, \frac{\delta}{N_L})} + \sqrt{2C_{S,i} L_i K_i(\rho, \pi, \frac{\delta}{N_L})}^{\frac{3}{2}}$,

or $\mathcal{U}_i(\rho) := \sqrt{\frac{N_L \bar{D}}{\delta} \left(2 \frac{C_{P,i}}{m_i} \mathbb{E}_{\boldsymbol{\theta} \sim \pi} \left[\|\hat{\nabla}_{\mathbf{x}} \ell_i(\boldsymbol{\theta})\|_2^2 \right] + \sqrt{2} \frac{C_{P,i} L_i}{m_i} K_i(\pi, \pi, \frac{\delta}{N_L})^{\frac{1}{2}} \right)}$ for Sobolev or Poincaré bounds, respectively. $\mathcal{U}^{\text{S}}(\rho)$ is the RHS term of inequalities 7 or 9.

Now a natural question may rise: which is the relevant training objective from these constraints? Practically, there is no guarantee that reducing the bound on $\mathcal{R}_{\text{PIML}}^{\text{S}}(\rho)$ will also reduce the bound on the target true risk $\mathcal{R}_{\text{PIML}}(\rho)$. Indeed, even if the learning algorithm successfully reduces the bound on $\mathcal{R}_{\text{PIML}}^{\text{S}}(\rho)$, it may increase the bound on the data-fidelity as well since the complexity is more easily inflated with smaller sample size. Therefore, for simplicity, we only use sample-weighted bound to tighten the union-bound after learning, rather than integrating it directly as a training objective. By combining the bounds over single losses, we derive the surrogate objectives (**bounding-aware**) in 10 and 11.

B.5 Implementations

Throughout the experiments, we mainly aim to verify the exploration ability of the self-bounding-aware algorithm, rather than to obtain state-of-the-art performance. For dataset generation, we uniformly sample 100k collocation points in 2D over the domains associated with each physical loss term: Ω for ℓ_d , Ω_0 for ℓ_i , and $\partial\Omega$ for ℓ_b . These are partitioned into prior, calibration, posterior, and test sets containing 10k, 20k, 30k, and 40k samples, respectively. For the data-fidelity loss, we instead sample 80k points, using 10k for calibration, 30k for the posterior set, and the remaining 40k for testing. In the unbalanced setting, we use a fixed subset consisting of the first m_d samples from the posterior set. For each benchmark, datasets are generated once and reused across all experimental configurations to ensure a consistent evaluation protocol.

We use a standard PINN with a two-dimensional input, three hidden layers of width 256 neurons, and a scalar output. Each hidden layer employs a tanh activation function. The resulting network contains approximately $d_\theta \approx 1.3 \times 10^5$ parameters. Accordingly, we choose the radius R such that $(3\sigma)^2 d_\theta \sim R^2 = 1$. We normalise the model’s input using mean and standard deviation computed from the calibration set of PDE loss. For Step 1, the prior model is initialised with $\frac{1}{\sqrt{\text{fan}_{in}}}$ -scaled uniform distribution, with fan_{in} corresponding to the input connections of the neurons of the considered layer, and then trained during $N_T = 30,000$ iterations for 1D-Wave and Convection, while $N_T = 10,000$ for 1D-Reaction. This is to ensure that the self-bounding-aware algorithm can still search for a posterior distribution distinct from the prior, rather than staying at an already good prior and learning nothing in the second stage. Then we estimate the constants by setting $N_{draw} = 10$, $k = 10$ and searching for τ within the range $1 - 10^4$. For each random seed, we train a single prior, which is then used both to estimate the constants and to initialise the posterior for all bounds in Stage 2. This ensures that all bounds use identical constants and initialisations, enabling a fair comparison.

During Step 2, to optimise the bound, we fix the confidence parameter $\delta = 0.05$, and the variance $\sigma^2 = 10^{-6}$ for both prior distribution π and posterior distribution ρ . The parameter of the posterior distribution is learned for $N_{T'} = 10,000$ iterations. We make use of Adam optimiser with a batch size of 300 for both stages. The learning rate is initialised at 10^{-3} for Stage 1 and 10^{-7} for Stage 2, with an exponential decay of 0.95 after every 1000 iterations. All experiments are implemented in PyTorch [30] and the optimization problem 52 is solved using `scipy.optimize.minimize` tools. The expected empirical risk is estimated via Monte Carlo simulation by sampling 100 models from the posterior distribution. The models are trained on a single NVIDIA RTX 5090 GPU.

B.6 Detailed results

Table 3 reports detailed results for the balanced setting with $m_d = 30k$. Among all methods, **Ours-Sob** consistently achieves the smallest bound values across all benchmarks. The KL divergences between the posterior and prior are generally larger for the Sobolev-type bounds, reflecting their weaker constraints compared to the Poincaré-type counterparts. In particular, **Ours-Sob**, which uses the total training size as the effective sample size, permits a wider optimization region and consequently attains substantially larger KL divergences. In nearly all cases, the bound values decrease after posterior learning, indicating that the self-bounding-aware algorithm effectively minimizes the target bound.

Tables 4 and 5 report detailed results for the unbalanced setting with $m_d = 300$. While the bounds only increase slightly for the 1D-Wave problem, they inflate much more rapidly for the other two problems. This behavior is primarily caused by the small training sample size in one partition, as well as the use of the constants of ℓ_{ic} for ℓ_d —which are orders of magnitude larger—to compensate for the absence of calibration data. Regarding Poincaré-type bounds, it is clear that **Ours-Poi.** achieves much lower bounds compared to **Ours-Poi._S** and $\bar{U}_{\text{Poi.}}$. This can be explained by the fact that union Poincaré bounds increase with a factor of $\sqrt{N_L}$, and the sample-weighted constraint (to obtain **Ours-Poi._S**) can partially compensate it. As a result, it is better to directly use the equally-weighted bound in inequality 8. Besides, with little improvement and in some cases even deteriorate, it indicates that with stricter constraint, it is more difficult for the learning algorithm to minimise the Poincaré-type bounds. In contrast, the algorithm remains effective at reducing the Sobolev-type bounds and the empirical risks simultaneously. Using the PAC-Bayes-Sobolev bound in Theorem 3.5 effectively helps to tighten the bound obtained by the baseline union approach. However, this gain is

less considerable compared to **Ours-Sob.** bounds obtained in the balanced setting. This suggests that integrating the sample-weighted constraint into the training objective might be of great interest.

Designing such objectives is generally nontrivial and often requires substantial effort. However, in physics-informed settings, the typical abundance of physics-based samples can be leveraged to derive tighter bounds in the unbalanced regime. In practice, the sample size associated with the physical losses can be made arbitrarily large. To take advantages from this, we can combine all physical losses into a single loss $\mathcal{R}_{\text{physics}}(\rho)$, for example $\mathcal{R}_{\text{physics}}(\rho) = \mathcal{R}_p(\rho) + \mathcal{R}_{ic}(\rho) + \mathcal{R}_b(\rho)$ in 1D-Reaction and Convection. As mentioned in Appendix B.4, we can obtain a bound on $\mathcal{R}_{\text{physics}}(\rho)$ in both balanced (direct result) and unbalanced settings (by solving the optimization problem 52). Informally, with probability at least $1 - \delta'$, where $\delta' \in (0, \delta)$, we can always obtain a bound of the form $\mathcal{R}_{\text{physics}}(\rho) \leq \hat{\mathcal{R}}_{\text{physics}}(\rho) + \mathcal{C}_{\text{physics}}(\delta')$. Then applying a union bound together with the bound on $\mathcal{R}_d(\rho)$, which holds with probability at least $1 - (\delta - \delta')$, yields a bound on $\mathcal{R}_{\text{PIML}}(\rho)$. Now, it is obvious that allocating a smaller confidence budget δ' to bound on $\mathcal{R}_{\text{physics}}(\rho)$ has only a limited effect on $\mathcal{C}_{\text{physics}}(\delta')$, due to the large associated sample size, while assigning a larger budget $\delta - \delta'$ to the data term mitigates the inflation of the bound induced by the small value of m_d . To validate this idea, we employ the PAC-Bayes-Sobolev bound in Theorem 3.5 with $\delta' = \delta/2$ and obtain a Sobolev-type bound of 1.61 ± 0.19 on 1D-Wave when $m_d = 2$. This bound is substantially tighter than **Ours-Sob.** (1.75 in Table 1). Furthermore, the improvement achieved by this strategy is considerably larger than that obtained by solving the optimization problem in 52 (i.e., from 1.76 of $\mathbf{U}_{\text{Sob.}}$ to 1.61, compared to 1.76 to 1.75).

Table 3: Results for the balanced setting with $m_d = 30k$. Reported values are averages and standard deviations over 5 runs for the empirical (Emp.) risks, KL divergence, and bound values before ($\mathcal{U}(\pi)$) and after ($\mathcal{U}(\rho)$) Stage 2 of Algorithm 1. Blue numbers indicate that the bound decreases after training.

Dataset	Metric	Ours-Sob.	Ours-Poi.	$\mathcal{U}_{\text{Sob.}}$	$\mathcal{U}_{\text{Poi.}}$	
1D-Wave	Emp. Train Risk	$\hat{\mathcal{R}}_d(\rho)$	(1.17±0.11)e-4	(1.24±0.18)e-4	(1.22±0.14)e-4	(1.25±0.19)e-4
		$\hat{\mathcal{R}}_p(\rho)$	(4.05±0.42)e-1	(4.33±0.40)e-1	(4.14±0.45)e-1	(4.36±0.39)e-1
		$\hat{\mathcal{R}}_{ic}(\rho)$	(1.37±0.52)e-4	(1.54±0.92)e-4	(1.47±0.71)e-4	(1.55±0.94)e-4
		$\hat{\mathcal{R}}_{ig}(\rho)$	(1.00±0.04)e-2	(1.02±0.10)e-2	(1.04±0.07)e-2	(1.03±0.10)e-2
		$\hat{\mathcal{R}}_{b_1}(\rho)$	(1.05±0.11)e-4	(1.15±0.12)e-4	(1.10±0.14)e-4	(1.15±0.13)e-4
		$\hat{\mathcal{R}}_{b_2}(\rho)$	(1.14±0.06)e-4	(1.18±0.14)e-4	(1.18±0.09)e-4	(1.18±0.14)e-4
		$\sum \hat{\mathcal{R}}_{\text{train}}(\rho)$	(4.16±0.42)e-1	(4.44±0.40)e-1	(4.25±0.46)e-1	(4.46±0.39)e-3
	Emp. Test Risk	$\hat{\mathcal{R}}_d(\rho)$	(1.15±0.11)e-4	(1.24±0.19)e-4	(1.20±0.14)e-4	(1.25±0.19)e-4
		$\hat{\mathcal{R}}_p(\rho)$	(4.11±0.52)e-1	(4.35±0.40)e-1	(4.24±0.51)e-1	(4.37±0.39)e-1
		$\hat{\mathcal{R}}_{ic}(\rho)$	(1.54±0.92)e-4	(1.54±0.92)e-4	(1.49±0.71)e-4	(1.54±0.93)e-4
		$\hat{\mathcal{R}}_{ig}(\rho)$	(9.92±1.15)e-3	(1.02±0.10)e-2	(1.05±0.10)e-2	(1.02±0.10)e-2
		$\hat{\mathcal{R}}_{b_1}(\rho)$	(1.10±0.12)e-4	(1.15±0.12)e-4	(1.15±0.13)e-4	(1.16±0.13)e-4
		$\hat{\mathcal{R}}_{b_2}(\rho)$	(1.11±0.11)e-4	(1.18±0.14)e-4	(1.17±0.14)e-4	(1.18±0.14)e-4
		$\sum \hat{\mathcal{R}}_{\text{test}}(\rho)$	(4.22±0.52)e-1	(4.48±0.48)e-1	(4.25±0.46)e-1	(4.46±0.39)e-3
	KL	3.20±0.84	(9.74±5.94)e-3	(9.67±1.77)e-1	(2.09±1.21)e-3	
	$\mathcal{U}(\pi)$	(7.06±1.56)e-1	(7.20±1.18)e-1	(7.11±1.56)e-1	1.13±0.24	
	$\mathcal{U}(\rho)$	(6.76±1.48)e-1	(7.14±1.13)e-1	(6.80±1.45)e-1	1.12±0.24	
	$\mathcal{U}(\pi) - \mathcal{U}(\rho)$	3.0e-2	6e-3	3.1e-2	1.0e-2	
1D-Reaction	Emp. Train Risk	$\hat{\mathcal{R}}_d(\rho)$	(2.66±0.41)e-3	(2.99±0.47)e-3	(2.79±0.43)e-3	(3.00±0.47)e-3
		$\hat{\mathcal{R}}_p(\rho)$	(1.09±0.03)e-3	(1.21±0.15)e-3	(1.08±0.03)e-3	(1.26±0.21)e-3
		$\hat{\mathcal{R}}_{ic}(\rho)$	(6.92±0.24)e-5	(8.03±1.81)e-5	(6.89±0.25)e-5	(8.43±2.46)e-5
		$\hat{\mathcal{R}}_b(\rho)$	(2.97±0.15)e-4	(3.69±0.94)e-4	(2.97±0.16)e-4	(3.97±1.41)e-4
			$\sum \hat{\mathcal{R}}_{\text{train}}(\rho)$	(4.12±0.42)e-3	(4.65±0.50)e-3	(4.24±0.44)e-3
	Emp. Test Risk	$\hat{\mathcal{R}}_d(\rho)$	(2.60±0.40)e-3	(2.89±0.45)e-3	(2.73±0.42)e-3	(2.91±0.45)e-3
		$\hat{\mathcal{R}}_p(\rho)$	(1.10±0.03)e-3	(1.10±0.01)e-3	(1.08±0.03)e-3	(1.15±0.07)e-3
		$\hat{\mathcal{R}}_{ic}(\rho)$	(6.94±0.25)e-5	(7.20±0.41)e-5	(6.91±0.25)e-5	(7.60±1.07)e-5
		$\hat{\mathcal{R}}_b(\rho)$	(2.98±0.16)e-4	(3.14±0.14)e-4	(2.97±0.16)e-4	(3.38±0.52)e-4
			$\sum \hat{\mathcal{R}}_{\text{test}}(\rho)$	(4.06±0.41)e-3	(4.37±0.45)e-3	(4.18±0.45)e-3
		KL	11.07±2.39	(2.34±2.87)e-2	(4.67±2.90)e-1	(5.91±6.53)e-3
		$\mathcal{U}(\pi)$	(7.39±1.17)e-3	(7.64±1.45)e-3	(7.99±1.28)e-3	(1.18±0.25)e-2
		$\mathcal{U}(\rho)$	(7.28±1.23)e-3	(7.54±1.40)e-3	(7.59±1.10)e-3	(1.18±0.25)e-2
		$\mathcal{U}(\pi) - \mathcal{U}(\rho)$	1.1e-4	1e-4	4.0e-4	0.
Convection	Emp. Train Risk	$\hat{\mathcal{R}}_d(\rho)$	(2.76±0.86)e-2	(2.89±0.89)e-2	(2.80±0.86)e-2	(2.89±0.89)e-2
		$\hat{\mathcal{R}}_p(\rho)$	(2.67±0.40)e-2	(3.81±0.72)e-2	(2.76±0.35)e-2	(3.96±0.75)e-2
		$\hat{\mathcal{R}}_{ic}(\rho)$	(3.07±0.17)e-4	(4.71±2.49)e-4	(3.34±0.63)e-4	(4.76±2.56)e-4
		$\hat{\mathcal{R}}_b(\rho)$	(1.18±0.34)e-3	(1.14±0.28)e-3	(1.17±0.34)e-3	(1.14±0.28)e-3
			$\sum \hat{\mathcal{R}}_{\text{train}}(\rho)$	(5.58±1.11)e-2	(6.86±1.57)e-2	(5.71±1.09)e-2
	Emp. Test Risk	$\hat{\mathcal{R}}_d(\rho)$	(2.76±0.84)e-2	(2.86±0.87)e-2	(2.78±0.85)e-2	(2.87±0.87)e-2
		$\hat{\mathcal{R}}_p(\rho)$	(2.71±0.35)e-2	(3.45±0.61)e-2	(2.77±0.36)e-2	(3.68±0.67)e-2
		$\hat{\mathcal{R}}_{ic}(\rho)$	(3.24±0.53)e-4	(4.54±2.43)e-4	(3.34±0.63)e-4	(4.66±2.62)e-4
		$\hat{\mathcal{R}}_b(\rho)$	(1.17±0.34)e-3	(1.15±0.29)e-3	(1.17±0.34)e-3	(1.14±0.28)e-3
			$\sum \hat{\mathcal{R}}_{\text{test}}(\rho)$	(5.61±1.03)e-2	(6.47±1.43)e-2	(5.70±1.07)e-2
		KL	17.30±9.80	(5.83±3.28)e-1	10.30±4.70	(1.04±0.55)e-2
		$\mathcal{U}(\pi)$	(8.88±1.85)e-2	(9.26±2.40)e-2	(9.55±2.13)e-2	(1.28±0.34)e-1
		$\mathcal{U}(\rho)$	(7.64±1.14)e-2	(9.00±2.27)e-2	(8.31±1.49)e-2	(1.27±0.32)e-1
		$\mathcal{U}(\pi) - \mathcal{U}(\rho)$	1.24e-2	2.7e-3	1.24e-2	1e-3

Table 4: Results for Poincaré bounds in the unbalanced setting with $m_d = 300$. Reported values are averages and standard deviations over 5 runs for the empirical (Emp.) risks, KL divergence, and bound values before ($\mathcal{U}(\pi)$) and after ($\mathcal{U}(\rho)$) Stage 2 of Algorithm 1. **Blue** and **red** numbers indicate decreases and increases in the bound after training, respectively.

Dataset	Metric	Ours-Poi.	Ours-Poi. _S	U _{Poi.}	
1D-Wave	Emp. Train Risk	$\hat{\mathcal{R}}_d(\rho)$	(1.25±0.22)e-4	(1.25±0.22)e-4	
		$\hat{\mathcal{R}}_p(\rho)$	(4.33±0.39)e-1	(4.36±0.39)e-1	
		$\hat{\mathcal{R}}_{ic}(\rho)$	(1.54±0.92)e-4	(1.55±0.94)e-4	
		$\hat{\mathcal{R}}_{ig}(\rho)$	(1.02±0.09)e-2	(1.03±0.10)e-2	
		$\hat{\mathcal{R}}_{b_1}(\rho)$	(1.15±0.12)e-4	(1.15±0.12)e-4	
		$\hat{\mathcal{R}}_{b_2}(\rho)$	(1.18±0.14)e-4	(1.18±0.14)e-4	
		$\sum \hat{\mathcal{R}}_{\text{train}}(\rho)$	(4.46±0.40)e-1	(4.48±0.39)e-1	
	Emp. Test Risk	$\hat{\mathcal{R}}_d(\rho)$	(1.24±0.16)e-4	(1.25±0.19)e-4	
		$\hat{\mathcal{R}}_p(\rho)$	(4.35±0.39)e-1	(4.38±0.39)e-1	
		$\hat{\mathcal{R}}_{ic}(\rho)$	(1.54±0.92)e-4	(1.54±0.93)e-4	
		$\hat{\mathcal{R}}_{ig}(\rho)$	(1.02±0.09)e-2	(1.02±0.10)e-2	
		$\hat{\mathcal{R}}_{b_1}(\rho)$	(1.15±0.12)e-4	(1.16±0.13)e-4	
		$\hat{\mathcal{R}}_{b_2}(\rho)$	(1.19±0.11)e-4	(1.18±0.14)e-4	
		$\sum \hat{\mathcal{R}}_{\text{test}}(\rho)$	(4.46±0.40)e-1	(4.48±0.39)e-1	
	KL	(9.54±5.52)e-3	(1.67±0.83)e-3		
	$\mathcal{U}(\pi)$	(7.22±1.18)e-1	(8.07±1.14)e-1	1.21±0.24	
	$\mathcal{U}(\rho)$	(7.16±1.12)e-1	(8.03±1.08)e-1	1.21±0.23	
	$\mathcal{U}(\pi) - \mathcal{U}(\rho)$	6e-3	4e-3	0.	
1D-Reaction	Emp. Train Risk	$\hat{\mathcal{R}}_d(\rho)$	(3.22±0.49)e-3	(3.22±0.49)e-3	
		$\hat{\mathcal{R}}_p(\rho)$	(1.31±0.27)e-3	(1.32±0.28)e-3	
		$\hat{\mathcal{R}}_{ic}(\rho)$	(8.81±3.04)e-5	(8.83±3.10)e-5	
		$\hat{\mathcal{R}}_b(\rho)$	(4.23±1.83)e-4	(4.26±1.87)e-4	
		$\sum \hat{\mathcal{R}}_{\text{train}}(\rho)$	(5.04±0.65)e-3	(5.05±0.66)e-3	
	Emp. Test Risk	$\hat{\mathcal{R}}_d(\rho)$	(2.93±0.47)e-3	(2.94±0.47)e-3	
		$\hat{\mathcal{R}}_p(\rho)$	(1.29±0.22)e-3	(1.29±0.23)e-3	
		$\hat{\mathcal{R}}_{ic}(\rho)$	(8.57±2.57)e-5	(8.60±2.63)e-5	
		$\hat{\mathcal{R}}_b(\rho)$	(4.02±1.62)e-4	(4.04±1.66)e-4	
		$\sum \hat{\mathcal{R}}_{\text{test}}(\rho)$	(4.71±0.59)e-3	(4.72±0.61)e-3	
		KL	(2.62±2.60)e-4	(8.92±7.74)e-5	
		$\mathcal{U}(\pi)$	(7.06±1.20)e-2	(1.36±0.23)e-1	(1.37±0.24)e-1
		$\mathcal{U}(\rho)$	(7.06±1.20)e-2	(1.36±0.23)e-1	(1.38±0.24)e-1
		$\mathcal{U}(\pi) - \mathcal{U}(\rho)$	0.	0.	-1e-3
Convection	Emp. Train Risk	$\hat{\mathcal{R}}_d(\rho)$	(2.90±0.98)e-2	(2.90±0.98)e-2	
		$\hat{\mathcal{R}}_p(\rho)$	(4.08±0.77)e-2	(4.08±0.77)e-2	
		$\hat{\mathcal{R}}_{ic}(\rho)$	(4.79±2.59)e-4	(4.79±2.59)e-4	
		$\hat{\mathcal{R}}_b(\rho)$	(1.14±0.28)e-3	(1.14±0.28)e-3	
		$\sum \hat{\mathcal{R}}_{\text{train}}(\rho)$	(7.14±1.70)e-2	(7.15±1.70)e-2	
	Emp. Test Risk	$\hat{\mathcal{R}}_d(\rho)$	(2.93±0.47)e-2	(2.87±0.87)e-2	
		$\hat{\mathcal{R}}_p(\rho)$	(4.08±0.80)e-2	(4.08±0.80)e-2	
		$\hat{\mathcal{R}}_{ic}(\rho)$	(4.77±2.75)e-4	(4.77±2.75)e-4	
		$\hat{\mathcal{R}}_b(\rho)$	(1.13±0.27)e-3	(1.13±0.27)e-3	
		$\sum \hat{\mathcal{R}}_{\text{test}}(\rho)$	(7.11±1.62)e-2	(7.11±1.62)e-2	
		KL	(9.52±4.20)e-6	(3.42±1.11)e-6	
		$\mathcal{U}(\pi)$	3.09±1.21	5.96±2.05	6.15±2.41
		$\mathcal{U}(\rho)$	3.09±1.21	5.97±2.06	6.15±2.42
		$\mathcal{U}(\pi) - \mathcal{U}(\rho)$	0.	-1e-2	0.

Table 5: Results for Sobolev bounds in the unbalanced setting with $m_d = 300$. Reported values are averages and standard deviations over 5 runs for the empirical (Emp.) risks, KL divergence, and bound values before ($\mathcal{U}(\pi)$) and after ($\mathcal{U}(\rho)$) Stage 2 of Algorithm 1. **Blue** and **red** numbers indicate decreases and increases in the bound after training, respectively.

Dataset	Metric	Ours-Sob.	$\mathcal{U}_{\text{Sob.}}$	
1D-Wave	Emp. Train Risk	$\hat{\mathcal{R}}_d(\rho)$	(1.15±0.10)e-4	
		$\hat{\mathcal{R}}_p(\rho)$	(4.10±0.46)e-1	
		$\hat{\mathcal{R}}_{ic}(\rho)$	(1.33±0.46)e-4	
		$\hat{\mathcal{R}}_{ig}(\rho)$	(1.00±0.04)e-2	
		$\hat{\mathcal{R}}_{b_1}(\rho)$	(1.06±0.10)e-4	
		$\hat{\mathcal{R}}_{b_2}(\rho)$	(1.13±0.05)e-4	
		$\sum \hat{\mathcal{R}}_{\text{train}}(\rho)$	(4.23±0.46)e-1	
	Emp. Test Risk	$\hat{\mathcal{R}}_d(\rho)$	(1.15±0.11)e-4	
		$\hat{\mathcal{R}}_p(\rho)$	(4.24±0.51)e-1	
		$\hat{\mathcal{R}}_{ic}(\rho)$	(1.38±0.48)e-4	
		$\hat{\mathcal{R}}_{ig}(\rho)$	(1.05±0.10)e-2	
		$\hat{\mathcal{R}}_{b_1}(\rho)$	(1.12±0.11)e-4	
		$\hat{\mathcal{R}}_{b_2}(\rho)$	(1.12±0.13)e-4	
		$\sum \hat{\mathcal{R}}_{\text{test}}(\rho)$	(4.23±0.46)e-1	
	KL	1.82±0.48		
	$\mathcal{U}(\pi)$	(7.28±1.54)e-1	(7.36±1.55)e-1	
	$\mathcal{U}(\rho)$	(7.01±1.52)e-1	(7.08±1.53)e-1	
	$\mathcal{U}(\rho)$	2.7e-2	2.8e-2	
1D-Reaction	Emp. Train Risk	$\hat{\mathcal{R}}_d(\rho)$	(3.11±0.49)e-3	
		$\hat{\mathcal{R}}_p(\rho)$	(1.21±0.10)e-3	
		$\hat{\mathcal{R}}_{ic}(\rho)$	(7.60±0.92)e-5	
		$\hat{\mathcal{R}}_b(\rho)$	(3.32±0.40)e-4	
		$\sum \hat{\mathcal{R}}_{\text{train}}(\rho)$	(4.72±0.44)e-3	
	Emp. Test Risk	$\hat{\mathcal{R}}_d(\rho)$	(2.85±0.46)e-3	
		$\hat{\mathcal{R}}_p(\rho)$	(1.21±0.10)e-3	
		$\hat{\mathcal{R}}_{ic}(\rho)$	(7.62±0.92)e-5	
		$\hat{\mathcal{R}}_b(\rho)$	(3.32±0.40)e-4	
		$\sum \hat{\mathcal{R}}_{\text{test}}(\rho)$	(4.46±0.41)e-3	
		KL	(2.38±0.93)e-1	
		$\mathcal{U}(\pi)$	(5.85±0.64)e-2	(5.89±0.65)e-2
		$\mathcal{U}(\rho)$	(5.77±0.61)e-2	(5.81±0.62)e-2
		$\mathcal{U}(\pi) - \mathcal{U}(\rho)$	8e-4	8e-2
Convection	Emp. Train Risk	$\hat{\mathcal{R}}_d(\rho)$	(2.88±0.97)e-2	
		$\hat{\mathcal{R}}_p(\rho)$	(4.01±0.80)e-2	
		$\hat{\mathcal{R}}_{ic}(\rho)$	(4.56±2.10)e-4	
		$\hat{\mathcal{R}}_b(\rho)$	(1.13±0.28)e-3	
		$\sum \hat{\mathcal{R}}_{\text{train}}(\rho)$	(7.04±1.73)e-2	
	Emp. Test Risk	$\hat{\mathcal{R}}_d(\rho)$	(2.84±0.87)e-2	
		$\hat{\mathcal{R}}_p(\rho)$	(4.01±0.80)e-2	
		$\hat{\mathcal{R}}_{ic}(\rho)$	(4.56±2.12)e-4	
		$\hat{\mathcal{R}}_b(\rho)$	(1.13±0.28)e-3	
		$\sum \hat{\mathcal{R}}_{\text{test}}(\rho)$	(7.01±1.62)e-2	
		KL	(3.16±2.82)e-1	
		$\mathcal{U}(\pi)$	2.29±0.88	2.28±0.88
		$\mathcal{U}(\rho)$	2.24±0.85	2.25±0.85
		$\mathcal{U}(\pi) - \mathcal{U}(\rho)$	4e-2	3e-2

Table 6: Comparison of the expected empirical risk under our posterior and under a Gaussian distribution centered at a deterministically NTK-trained model using the full training data (prior and posterior datasets combined).

Dataset	Emp. Test Risk	Ours-Sob.	NTK-60k
1D-Wave	$\hat{\mathcal{R}}_d(\rho)$	$(1.15 \pm 0.11)e-4$	$(9.77 \pm 0.45)e-5$
	$\hat{\mathcal{R}}_p(\rho)$	$(4.11 \pm 0.52)e-1$	$(3.97 \pm 0.29)e-1$
	$\hat{\mathcal{R}}_{ic}(\rho)$	$(1.54 \pm 0.92)e-4$	$(1.09 \pm 0.05)e-4$
	$\hat{\mathcal{R}}_{ig}(\rho)$	$(9.92 \pm 1.15)e-3$	$(1.04 \pm 0.12)e-2$
	$\hat{\mathcal{R}}_{b_1}(\rho)$	$(1.10 \pm 0.12)e-4$	$(1.00 \pm 0.05)e-4$
	$\hat{\mathcal{R}}_{b_2}(\rho)$	$(1.11 \pm 0.11)e-4$	$(1.03 \pm 0.06)e-4$
	$\sum \hat{\mathcal{R}}_{\text{test}}(\rho)$	$(4.22 \pm 0.52)e-1$	$(4.08 \pm 0.30)e-1$
1D-Reaction	$\hat{\mathcal{R}}_d(\rho)$	$(2.60 \pm 0.40)e-3$	$(6.74 \pm 0.28)e-5$
	$\hat{\mathcal{R}}_p(\rho)$	$(1.10 \pm 0.03)e-3$	$(1.18 \pm 0.07)e-3$
	$\hat{\mathcal{R}}_{ic}(\rho)$	$(6.94 \pm 0.25)e-5$	$(7.25 \pm 0.28)e-5$
	$\hat{\mathcal{R}}_b(\rho)$	$(2.98 \pm 0.16)e-4$	$(3.10 \pm 0.25)e-4$
	$\sum \hat{\mathcal{R}}_{\text{test}}(\rho)$	$(4.06 \pm 0.41)e-3$	$(1.63 \pm 0.09)e-3$
Convection	$\hat{\mathcal{R}}_d(\rho)$	$(2.76 \pm 0.84)e-2$	$(3.39 \pm 0.27)e-4$
	$\hat{\mathcal{R}}_p(\rho)$	$(2.71 \pm 0.35)e-2$	$(1.21 \pm 0.36)e-2$
	$\hat{\mathcal{R}}_{ic}(\rho)$	$(3.24 \pm 0.53)e-4$	$(3.13 \pm 0.13)e-4$
	$\hat{\mathcal{R}}_b(\rho)$	$(1.17 \pm 0.34)e-3$	$(2.79 \pm 0.66)e-4$
	$\sum \hat{\mathcal{R}}_{\text{test}}(\rho)$	$(5.61 \pm 1.03)e-2$	$(1.30 \pm 0.37)e-2$

For completeness, we also compare our self-bounding-aware algorithm against the best results obtained by a state-of-the-art PINN training approach based on the neural tangent kernel (NTK) [41]. Since our method outputs a posterior distribution rather than a single deterministic model, we compare the expected empirical test risk under our posterior with that obtained from a Gaussian distribution centered at the deterministic NTK-trained model. The NTK model is trained for both 60k iterations on the full training set, obtained by combining the prior and posterior datasets. In contrast, our self-bounding-aware algorithm uses a total of only 40k iterations for 1D-Wave and 1D-Convection, and 20k iterations for 1D-Reaction.

The results are reported in Table 6 under **Ours-Sob.**. Overall, the NTK-based method achieves lower risks across the three benchmarks. Nevertheless, for 1D-Wave, **Ours-Sob.** attains slightly lower risks on the initial condition (IC) losses. For the more challenging 1D-Reaction and 1D-Convection problems, the NTK method significantly outperforms our approach, particularly on the data-fidelity term. However, while our objective was not to provide the best numerical results but rather a novel principled statistical framework for PIML, our posterior still achieves PDE residual risks of the same order of magnitude, and in some cases even lower values, notably for all physical losses in 1D-Reaction.

One possible explanation is that, for problems whose solutions exhibit sharp transitions or high-frequency structures, sufficiently long training can substantially reduce the approximation error of deterministic models. In contrast, it may be inherently difficult to further reduce the PDE residual in order to accurately capture fine-scale variations. Consequently, when such highly trained models are used as priors, the self-bounding-aware algorithm may have limited room to further tighten the bound. This opens the door for developing new ways to integrate physics priors in PAC-Bayes and more efficient (self-bounding)-algorithms.

C Limitations

This paper presents a PAC-Bayesian analysis for physics-informed machine learning and provides both generalisation guarantees and practical algorithms, supported by extensive experiments in three benchmarks. Despite promising results with tight bounds and intuitive results, there are still several limitations. Regarding theoretical analysis, the Poincaré bounds with χ^2 -divergence and

prior-dependent complexity is less flexible and difficult to be minimised in practice. On the other hand, it remains unclear how the physical constraint impacts the generalisation behavior of the data-fidelity loss. In the experimental part, the estimation of constants, although being effective, is stochastic and deeply depends on the number of draw N_{draw} , requiring random seed to obtain repetitive results. The use of ℓ_{ic} 's constants to alleviate observational data scarcity is clearly suboptimal and is a factor that inflates the bound. Finding an alternative deterministic approach to estimate the constants and avoid this looseness is one of the main open questions. Finally, the surrogate objective in the case of unbalanced setting does not directly integrate the constraint offer by the sample-centric bound, and designing such objectives might be a direction for future works.

D Related works

Generalisation of PIML. Despite tremendous empirical success, the generalisation of physics-informed machine learning (PIML) methods remains an open question that requires further study. A common line of work focuses on the convergence of physics informed models to the PDE solution [38, 12]. In particular, [12] addresses overfitting of PINNs by introducing a Sobolev regularisation term to enforce estimator regularity and show consistency and strong convergence properties. Other works derive approximation error bounds under stability assumptions on the underlying PDEs [35, 28]. Several papers study generalisation via (local) Rademacher complexity [24, 26, 42]; notably, [42] obtains generalisation bounds for second order elliptic PDEs by adopting a multi-task perspective and assuming the underlying solutions lie in Barron or Sobolev spaces. [10, 11] treat the PIML problem as a kernel regression task and use Fourier methods to construct tractable estimators with quantified convergence rates. [36] views physical loss terms as a form of regularisation in addition to data-fidelity loss and shows that, under a knowledge alignment assumption (i.e., the regulariser is approximately zero at the true solution), the estimator converges at a faster rate. Together, these works highlight the importance of encoding prior knowledge about the physical system—via regularity, stability, or data-physics alignment—to establish generalisation guarantees for approximation error or the total PIML loss. In the same vein, we establish a connection between generalisation, data, and physical regularity by employing a PAC-Bayesian framework to derive bounds based on input gradient complexity, and empirically show that, under sufficient regularity of the true solution, tight bounds can be obtained even in low data regimes.

PAC-Bayesian analysis for PIML. PAC-Bayes theory has emerged as a powerful framework for analysing modern machine learning models through data-dependent probabilistic guarantees that balance empirical risk and model complexity via information-theoretic divergences [1, 17, 22]. While early PAC-Bayesian analyses primarily focused on bounded-loss classification settings, more recent works have extended the framework to regression and heavy-tailed losses through higher-order moment control [19, 23], assumptions on the cumulant generating function (CGF) [6, 33], and structural assumptions on the data distribution [37, 18]. These advances are particularly relevant for physics-informed machine learning (PIML), where losses induced by PDE residuals or physical constraints are typically unbounded and may exhibit complex tail behaviour. Moreover, PAC-Bayes naturally accommodates prior physical knowledge through structured priors and constrained hypothesis spaces. More recently, a line of work has explored model-dependent assumptions leading to generalisation bounds that incorporate regularisation terms based on parameter norms [16], parameter gradients [21], and input gradients [14, 6]. Closest to our work, [6] derive empirical PAC-Bayes bounds with input-gradient-scaled complexity terms. However, their analysis focuses on a single loss function, and it remains unclear how the resulting constants can be estimated in practical PIML settings. In contrast, we adopt a multi-task perspective, under two different smoothness assumptions, to derive joint bounds that are tighter than standard union-bound constructions. Furthermore, to the best of our knowledge, our work is among the first to provide both PAC-Bayesian generalisation guarantees and a complete practical procedure for learning and computing the bounds in PIML settings.